Stagnant slab: A review

Yoshio FUKAO. Masayuki OBAYASHI, Tomoeki, NAKAKUKI and Deep slab project group*

*Deep slab project group includes Hisashi UTADA, Daisuke SUETSUGU, Tetsuo IRIFUNE, Eiji OHTANI, Shoichi YOSHIOKA, Hajime SHIOBARA, Kei HIROSE and Hitoshi KAWAKATSU

Abstract

Stagnant slab is a subducted slab of oceanic lithosphere subhorizontally deflected above, across or below the 660-km discontinuity. This phenomenon has now been widely recognized beneath subduction zones around the circum Pacific and in the Mediterranean. Collaboration of seismic and electromagnetic observations, mineral physics measurements, and geodynamic modeling begins to provide a consistent picture of stagnant slab.

1. Introduction

Near-horizontal deflection of subducted slab has been first detected from a travel time analysis by Okino et al. (1989) and imaged in the transition zone beneath Japan by van der Hilst et al. (1991), Fukao et al. (1992) and van der Hilst et al. (1993) through their P-wave travel time tomography. Fukao et al (1992) showed that such deflection or flattering occurs either above (as in Japan) or below (as in Indonesia) the 660-km discontinuity in the western Pacific. Fukao et al. (2001) made an extensive review of tomographic models of deeply seated slabs around the Circum Pacific to conclude that subducted slabs tend to be, in general, once horizontally flattened at various depths in a range roughly between 400 and 1000 km. They called a slab in this tendency “stagnant slab”. The subsequent development in this direction includes imaging of the flattened slab of the Mediterranean lithosphere in the transition zone under south Europe (Priromallo and Morelli, 2003; Marone et al., 2004; Schmid et al., 2006), that

of the Cocos to-Farallon plate under south Mexico (Gorbatov and Fukao, 2005) and the remnant flattened slab of the Farallon plate under south North America (Van der Lee and Nolet, 1997; Schmid et al., 2002; Lei and Zhao, 2006).

Figure 1 shows a wide-angle slice of the P-wave tomographic model of the Earth's mantle (Fukao et al., 2001). This slice displays the stagnant slab of the Pacific plate behind the Honshu arc, which apparently lies on the 660-km discontinuity. The lowermost mantle under this stagnant slab image is marked by extensive high velocity anomalies. These deepest anomalies and those at somewhat shallower depths under the northwestern Pacific and eastern Eurasia have been interpreted as the remnants of subducted slabs once falling through the lower mantle and now residing in the deep or deepest lower mantle (Fukao et al., 1992; Van der Voo et al.,:1999). The two obvious examples of subducted slabs now falling through the lower mantle yet not reaching its bottom are the Tethyan lithosphere (van der Hilst et al., 1997; Grand et al., 1997; Bijwaard et al., 1998; Replumaz et al., 2004; Hafkenscheid et al., 2006) and the Farallon lithosphere (van der Hilst et al., 1997; Grand et al., 1997; Bijwaard et al., 1998; Zhao, 2004; Lei and Zhao, 2006).

Our questions in this study are addressed to how thermally and compositionally anomalous stagnant slab is, why subducted slab tends to be once flattened above or below the 660-km discontinuity and what happens to a slab falling into the lower mantle. .

.

2. Stagnant slab image behind the Japanese arc

Because of the abundant seismic stations available in Japan and China, the stagnant slab behind the Japanese arc is especially suitable to detail its fine structure. By adding many regional P-wave travel time data of the Chinese networks to those reported to the International Seismological Center (ISC), Huang and Zhao (2006) were able to obtain sharper images of the flat

portion of the Pacific slab under east China. **Figure 2** shows the E-W vertical cross-sections of P wave velocity perturbations along latitudes 41°, 39° and 37°. The subducted slab of the Pacific plate is sharply deflected to horizontal when it hits the bottom of the upper mantle. The horizontal slab extends over a distance of 800 to 1000 km above the 660-km discontinuity. The uppermost mantle is significantly slow not only above the inclined Wadati-Benioff zone but also continent-ward all the way above the horizontally deflected slab. Lei and Zhao (2005) and Huang and Zhao (2006) called this extensive low velocity zone a "big wedge mantle" and emphasized its significance on surface tectonics, including intraplate seismicity and volcanism in east China, and its possible geodynamic link to slab-stagnation processes. Water may play a role in this linkage, the possible presence of which has been indicated by a long period magnetotelluric study (Ichiki et al., 2006) in a part of the upper mantle just above the stagnant slab of the same region.

Fukao et al. (2001) pointed out that the P wave high velocity images of stagnant slab from travel time tomography can be compared to the broad spreads of S wave high velocity anomaly at the corresponding depths in long-wavelength tomographic models from waveform inversion, such as S12WM13 (Su et al., 1994) and SAW12D (Li and Romanowicz, 1996). The spatial similarity between the positive P and S velocity anomalies in the transition zone has also been pointed out by Grand (2002) and Romanowicz (2003). High resolution tomographic studies using S wave travel time data, on the other hand, have not yielded stagnant slab images comparable in sharpness and intensity to those from P wave tomography. Widiyantoro et al (1999) made a joint inversion of P and S travel times by selecting data having common source and receiver for P and S arrivals. Their models showed substantial differences in the portions of stagnant slabs between P and S wave tomographic images. For example, the P wave image beneath the Izu-Bonin region showed a strong signature of stagnant slab but the S wave image did not. This point has been

elaborated by Gorbatov and Kennett (2002) and Kennett and Gorbatov (2004) who made joint tomography for bulk-sound and shear wave velocities using arrival times for paths with common source and receiver for P and S. **Figure 3** displays the vertical cross-section through the model of Gorbatov and Kennett (2003) across the Izu-Bonin and Ryukyu arcs along profile PP' shown in the map in Fig. 2. The downgoing part of the subducted slab is strongly anomalous in shear wave velocity but only slightly in bulk-sound velocity, while the horizontal portion is more anomalous in bulk-sound velocity than in shear velocity. This may imply that the thermal anomaly controls velocity anomalies of the downgoing portion while the compositional difference contributes significantly to the anomalies of the horizontal portion (Gorbatov and Kennett, 2003).

There is, however, some evidence that the horizontal portion is anomalously fast not only in P but also in S by such amounts as expected from the thermal effect. **Figure 4** shows the vertical P and transverse S broadband seismograms at stations in southwest Japan and China for the deep shock of June 03, 2002 that occurred at a depth of 494 km within the Izu-Bonin slab. (See Fig. 2 for the hypocenter.) In a distance range where the effect of the stagnant slab is significant, the visually picked P arrivals are significantly early relative to the reference travel time curve of iasp21 (Engdahl et al., 1998) in good agreement with those predicted from the three-dimensional (3D) P-wave model of Obayashi et al. (2006) (Sugioka et al., 2007). This model is converted to a 3D S-wave model using the P to S velocity ratio of the reference model iasp91 for the 1D part and choosing an appropriate value of $R = (dVs/Vs)/(dVp/Vp)$ for the laterally perturbed part, where dVp/Vp and dVs/Vs are fractional P and S velocity perturbations (Bolton and Masters, 2001). The resultant theoretical S arrivals are in good match with the observed S arrivals in a distance of our interest. The value of R (=1.7) is comparable to the transition zone average of R from global tomography (Bolton, 1996; Masters et al., 2000). This implies that

both P and S velocity anomalies associated with the stagnant slab may be explained primarily by a temperature anomaly of 300 to 400 K (Sugioka et al, 2007). Friederich (2003) used full waveforms of shear and surface waves to show that high shear-velocity subducting slabs along the west Pacific subduction zones are stagnating at the 660 beneath East Asia. Obviously more studies are needed to characterize stagnant slabs in the northwestern Pacific by S velocity anomaly or Vp/Vs ratio.

3. Thermal state of stagnant slab .

Some information about how stagnant slab is thermally anomalous comes from topography of the 660-km discontinuity near the stagnant slab. The global SS precursor study of Flanagan and Shearer (1998) showed that the depression of the 660-km boundary occurs most extensively in the northwestern Pacific where the depression is about 20 km. They explained this feature by the low temperature effect of horizontally flattened subducting slabs in the mantle transition zone. The simultaneous inversion for the S velocity distribution and the discontinuity topography by Gu et al. (2003) showed a 660-km depressions of the similar magnitude. On the other hand, regional studies using near-source S to P converted waves showed a greater slab-induced depression of up to 60 km beneath Izu-Bonin (Wicks and Richards, 1993; Castle and Creager, 1996). These studies have much higher resolution in the immediate vicinity of the subducting slabs than the global SS precursor studies but little resolution even slightly outside. More recent studies using near-station P to S converted waves begin to resolve the above apparent discrepancy in the magnitude of 660-km depression between the global SS-S studies and the near-source S to P conversion studies.

Figure 5 shows the tomographic maps in three depth ranges, (a)just above the 410-km discontinuity, (b)in the mid transition zone and (c)around the 660-km discontinuity, respectively (Obayashi et al., 2006). Strongly fast anomalies in (a) are associated with the downgoing part of the Izu-Bonin slab of the

Pacific plate. Those in (b) spread to horizontal most extensively in the transition zone and correspond to the stagnant part of a subducted slab. Those in (c) represent the bottoming part at the intersection of the downgoing and stagnant parts which can be seen all the way along the southern Kurile, Honshu and northern Bonin arcs. **Figure 6a** explains this situation by taking a tomographic cross-section across the Izu-Bonin along profile AA' in Fig. 5c, where the three distinct parts may be identified, the part downgoing through the upper mantle, the part bottoming the 660 and the part flattening above the 660, corresponding to the slab images in Figs. 5a, 5c and 5b, respectively.

Figure 6b shows the cross-section of the topography of the 660 along the same profile AA', which was obtained by a receiver function analysis of near-station S to P converted waves recorded by Hi-Net (a Japanese dense seismic network) (Niu et al., 2005). Depression is greatest in the bottoming part, about 30 km in agreement with 20 40 km obtained by Li et al. (2000). Depression decreases gradually in the flattened part with increasing distance away from the bottoming part. No depression occurs under the obliquely downgoing part. The similar image (the largest depression in the slab bottoming part and smaller depression in the flattened part) has also been obtained from a one-station receiver function analysis of P to S converted waves for the stagnant slab beneath east China, as illustrated in Fig. 5c (Li and Yuan, 2003), where the largest depression of the similar magnitude has also been obtained by Li et al. (2000) and Ai et al. (2003). The 660 depression in this tendency can be qualitatively interpreted as the low temperature effect of the stagnant slab on the phase decomposition of ringwoodite (a high pressure phase of the most dominant upper mantle constituent mineral). These results, along with the result of a differential travel time analysis of the post-cursors of the ScS family by Tono et al. (2005), have given a consistent interpretation for the apparent difference between the 660 topography from the global SS-S studies (relatively shallow depression below the slab-flattening part) and

the topography from the near-source S to P conversion studies (relatively deep depression in the slab-bottoming part).

The tomographic and topographic images at the 660 in Figs. 6a and 6b may be compared to each other more quantitatively. In **Fig. 6b** we superpose the tomographic profile at 660-km depth and the topographic profile of the 660. These two anomaly profiles are remarkably parallel to each other, especially in a region of topographic depression, where a fractional P-velocity perturbation can be converted to a discontinuity depression using a conversion factor of 20 km/%. This conversion factor may be further converted to a "seismological" Clapeyron slope, assuming that the 660 is the phase boundary of decomposition of ringwoodite (Levedev et al., 2002).

Figure 7 shows the result of the recent ultrasonic measurements of P- and S-velocities of ringwoodite and majorite at various pressures and temperatures corresponding 'directly' to those in the transition zone (Higo et al., 2007; Irifune et al., 2007), from which we estimated P- velocity of ringwoodite to be Vp=10.28 km/s at a reference state of 21 Ga and 1800 K. The values of dK/dT and dG/dT obtained by Higo et al. (2007), where K and G are bulk and shear moduli, are not significantly different from those obtained by Shinogeikin et al. (2003) and Mayama et al. (2005) using a Brillouin scattering technique and a resonant sphere technique, respectively, at much lower pressures and temperatures. We estimated from Fig.7 the temperature sensitivity of fractional P-velocity perturbation at the reference state to be $(dVp/Vp)/dT$≒-0.35 %/100K. Note a strong nonlinearity of S-velocity variation with pressure, which makes $(dVs/Vs)/dT$ and hence R at the reference state much larger than those estimated from data in a lower pressure range. This observation should have an important implication for interpreting tomographic images in the transition zone. With the above value $(dVp/Vp)/dT$, the observed maximum P-velocity anomaly of +1.5 % in the bottoming part of the subducted slab corresponds to a

temperature anomaly of about -400K and the conversion factor of 20km/% corresponds to a 'seismological' Clapeyron slope of about -2.5 MPa/K. In the above estimates we have ignored the anelsticity effect on $(dVp/Vp)/dT$ (Karato, 1997) because seismic attenuation is small in the subducting slab especially for P waves. The Clapeyron slope of about -2.5 MPa/K is not unreasonable for the decomposition of ringwoodite, as will be discussed later, and hence lends support to the idea that the 660 is broadly depressed by the low-temperature effect of the stagnant slab and in turn that seismic anomalies of the stagnant slab are primarily of thermal origin.

Another line of evidence for supporting the idea that seismic anomaly of stagnant slab is primarily of thermal origin comes from the comparison of the seismic and electrical images of the stagnant slab under south Europe. **Figure 8** shows the tomographic maps by Schmid et al. (2006) who made a joint inversion of P and S arrival time data and Rayleigh waveform data for the P, S and bulk sound velocity structures. Seismic perturbations roughly to the west of 20° E are dominated by the fast anomalies associated with the stagnant slab in the transition zone. No anomalies are found in the mid lower-mantle. Thus, the subducted slab of the Mediterranean lithosphere is stagnant above the 660 to the west of 20°E. The fractional P and S velocity changes, dVp/Vp and dVs/Vs, in the transition zone due mainly to this stagnant slab are 1.5-2.0 % and 3-4 %, respectively. The value of R is then 2.0, which is, according to Schmid et al. (2006), consistent with the theoretical estimate of Cammarano et al. (2003), The P, S and bulk sound velocity anomalies in the transition zone can be, according to Schmid et al. (2006), consistently explained by the temperatures of the stagnant slab 300-400 K lower than the average.

Figure 9a shows the tomographic map of electrical conductivity at a depth of 500 km $log\sigma/\sigma_{1D}$ based on the regional geomagnetic data in Europe where σ and σ_{1D} are the three-dimensional

electrical conductivity and its one-dimensional reference, respectively (Utada et al., 2007, in preparation). The stagnant slab is imaged as an extensive horizontal spread of low electrical conductivity in a depth range around 500 km depth. They converted this electrical conductivity anomaly distribution to the temperature anomaly distribution at 500 km depth, using the following relation based on the Arrhenius formuls with activation enthalpy H.

$$dT/T_{1D}=kT_{1D}/H\ ln\sigma/\sigma_{1D}$$

where k is Boltzman's constant and T_{1D} is an assumed temperature of 1750K at 500-km depth (see Fukao et al., (2004)). The experimental value of H of ringwoodite is taken from Xu et al. (2000). **Figure 9b** shows the temperature anomalies of the stagnant slab estimated with this value, which are on the order of -400K and on the lower end of the range (-300 to -400K) of the estimates from the seismic anomalies by Schmid et al. (2006).

According to Huang et al. (2005) the samples used by Xu et al. (1998), to which we referred, contain a small amount of water (about 0.03 Wt%). If the slab below south Europe contained a larger amount of water than this, the temperature sensitivity of electrical conductivity of the slab should be higher than one used here (Wang et al., 2006), and accordingly the temperature anomalies obtained here may be regarded as an overestimate. Our estimate is, however, consistent with the one-dimensional conductivity profile of Tarits et al. (2004) beneath French Alps (see Fig. 9a for the location), according to which the conductivity is anomalously low in the transition zone where a temperature of 350-450 K less than normal is estimated. Tarits et al. (2004) interpreted this result in terms of the subducted slab dehydrated before reaching the transition zone.

4. Stagnant slab and water in the transition zone

The experimentally determined Clapeyron slope of the

post-spinel phase change was originally on the order of -3 MPa/K (-2.8 MPa/K by Ito and Takahashi (1989), -3.0 MPa/K by Akaogi and Ito (1993), and -2.9 MPa/K: Irifune et al. (1998)). The recent measurements, however, give in general a more gentle slope ranging from -2 to -0.5 MPa/K (-2.0 MPa/K by Bina and Helffrich (1994), -0.4~-2.0 MPa/K by Katsura et al. (2003) and -1.3 MPa/K by Fei et al. (2004). Litasov et al. (2005a,b) determined a Clapeyron slope of . -0.5~-0.8 MPa/K for dry ringwoodite and -2MPa/K for hydrous ringwoodite. **Figure 10** summarizes their results (Litasov et al., 2006), where addition of water in ringwoodite makes the Clapeyron slope steeper and this effect should be much stronger at lower temperatures if the phase boundary is allowed to be a curved line on the P/T diagram (Litasov et al., 2006). The 'seismological' Clapeyron slope of -2.5 MPa/K estimated for the Izu-Bonin slab in a previous section may imply the presence of water in the slab, although the issue of experimental determination of the Clapeyron slope of ringwoodite has not yet been settled.

Water in the transition zone can be stored in wadsleyite and rigwoodite up to 3 wt.% (Inoue et al., 1995; Kohlstedt et al., 1996; see Bolfan-Casanova 2005, for review). Suetsugu et al. (2006) made a simultaneous inversion of the 660 topography and the P-velocity anomalies for temperature anomalies and water content anomalies. Using the same dataset as in Fig. 6, and by referring to the dVp/dT value of ringwoodite obtained by Sinogeikin et al. (2003) and the dVp/dw values of ringwoodite obtained by Inoue et al. (1998), Wang et al. (2003) and Jacobsen et al. (2004) where w is water content, (see Jacobsen and Smyth (2006) for the more recent results), they showed that with an assumed Clapeyron slope of -2 MPa/K, the bottoming part of the stagnant slab, which apparently overshoots the 660-km depth, is 400 to 500 K colder than the normal but is nothing anomalous in water content. Suetsugu et al. (2006) suggested relative enrichment in the transition zone surrounding the stagnant slab rather than in the stagnant slab itself. Such enrichment may be

feasible, if water is transported into deep upper mantle by a return flow in the overriding upper mantle, as seismologically identified by Kawakatsu and Watada (2007). Koyama et al. (2006) interpreted the EM tomography in the northwetern Pacific (Fukao et al., 2004) jointly with the seismic tomography and estimated the possible water content of about 0.3 Wt% or more in the transition zone above the stagnant slab beneath the Philippine Sea. At present there is little evidence that the slab in the transition zone is more enriched in water than the surrounding transition zone.

Richard et al. (2006) raised an intriguing question how water carried by a subducting slab behaves when it enters and dwells in the high-solubility transition zone. Water may be expelled from slabs entering the low-solubility lower mantle at 660 km depth, where hydrous ringwoodite and superhydrous phase *B* decompose (Ohtani et al., 2004; Komabayashi and Omori, 2006). Released water may then be percolated upward into the transition zone. The transition zone may be hydrated accordingly. In order for this percolation mechanism to be efficient, the released water has to be oversaturated in the high-solbility wadsleyite and ringwoodite. Another way to hydrate the transition zone is from dehydration of slabs stagnating in the transition zone (Karato et al., 2006). The slab containing water would potentially lose water by diffusive transport, which is complicated by the temperature contrast between the cold slab and the overlying warm mantle. The diffusion of water out of the slab and the diffusion of heat into the slab occur simultaneously and are coupled by the temperature-dependent water solubility. Through this double-diffusive mechanism, according to Richard et al. (2006), essentially 50-100% of the water in the slab is expelled into the transition zone for typical residence times, ~50 Ma, of slabs floating horizontally across the transition zone. Occurrence of this process over a relatively broad region (the extent of slab deflection) may allow for enhanced distribution of water through the transition zone.

5. Conditions for slab stagnation

Stagnant slab has often been discussed in conjunction with the post-spinel transition across the 660-km discontinuity (e.g., Fukao et al., 1992). The negative Clapeyron slope of this phase transformation tends to resist against straightforward subduction of slabs. Its role has been investigated extensively from the view point of thermal convection since Schubert and Turcotte (1971). Christensen and Yuen (1985) found that the convection pattern changes its mode depending on the Clapeyron slope, from the one-layered mode of convection to the two-layered mode across the intermittent mode. The intermittent mode is characterized by intermittent occurrence of non-stationary one-layered (or two-layered) convection during quasi-stationary two-layered (or one-layered) convection, invoking transient slab stagnation in the transition zone. More realistic convection modeling studies demonstrated that, with plausible values of the Clapeyron slope, the intermittent mode of mantle convection is possible (e.g., Machetel and Weber, 1991, 1997; Solheim and Peltier, 1994). This is also the case of the 3D box and spherical shell geometries (Honda et al, 1993; Tackley et al., 1993; Bunge et al., 1997).

Figure 11 shows the existent range of the intermittent mode in the *dP/dT* versus *Ra* diagram for a uniform viscosity mantle with 3D spherical shell geometry, where *dP/dT* is the Clapeyron slope at the 660 and *Ra* is the basal Rayleigh number which is defined for the system component heated from below. Half of the heating comes from the system component internally heated. The basal Rayleigh number covers a wide range up to more than 10^8, which is the highest value ever achieved for the 3D spherical shell convection modeling (Yamagishi et al., 2004). The recent experimental values of the Clapeyron slope are in a range from -2 to -0.5 MPa/K for dry ringwoodite, and <-2 MPa/K for wet ringwoodite, while the 'seismic' Clapeyron slope is in a range from -3.5 to -2 MPa/K (e.g., -3.3 MPa/K in Lebedov et al. (2002) and -2.5 MPa/K in the present study). If the basal Rayleigh number of the

Earth's mantle is in a range from 10^7 to 10^8 (e.g. Tackley et al., 1993), and if the transition zone is hydrated as implied by the 'seismic' Clapeyron slope, the mantle convection may be understood as in a state of the intermittent mode, although there are many factors that have been ignored in the above discussion.

Such factors include (1)one-sided subduction with trench retreat (Christensen, 1996), (2)temperature- and pressure-dependent viscosity (e.g. Karato and Wu, 1993), (3)slab-weakening due to grain size reduction after the phase transition (Rubie, 1984; Riedel and Karato, 1997; Yamazaki et al., 2005; Nishihara et al., 2006), (4)olivine metastability in a cold slab (Tetzlaff and Schmeling, 2000), (5)viscosity jump across the 660 (Gurnis and Hager, 1988; Mitrovica and Forte, 1997), (6)a thin low viscosity layer near the 660 (Ito and Sato, 1991; Forte et al., 1993), and (7)oceanic crust separation near the 660 (van Keken et al., 1996; Karato, 1997). Since it is not feasible at present to conduct 3D spherical shell modeling of convection by taking all of these factors into account, 2D numerical fluid simulation with its space restricted near a subduction zone has been attempted extensively (e.g. Čížková et al., 2002; Yoshioka and Sanshadokoro, 2002; Torii and Yoshioka, 2007; Tagawa et al., 2007).

Figures 12a, 12b and 12c show the effects of the first three factors among those listed above (Tagawa, 2007). One-sided subduction occurs in this model along a megathrust zone with history-dependent fault rheology. Trench migration is ensured by letting the side walls of the model space free in slip. Temperature- and pressure-dependence of viscosity is quoted from Karato and Wu (1993). Softening due to grain size reduction associated with phase transition is allowed in the colder part ($T<To$) of the slab at depths below the 410km transition. There is no viscosity jump across the 660. In Figs. 12a, 12b and 12c, the Clapeyron slope is -2, -3 and -1 MPa/K, and the critical temperature To is 1073, 1873 and 1073 K, respectively, although To of 1873 K is likely to be too

high to be realistic. The slab is deflected horizontally at depths across the 660 in Fig. 12a and below the 660 in Fig. 12c. In Fig. 12b the bottoming part of the downgoing slab sinks into the lower mantle as blob, leaving the horizontally deflected part above the 660. Thus, a variety of slab configuration arises without introducing any extra discontinuities at depths below 660km, as has been already demonstrated by Christensen (1996) and Čížková et al. (2002). For example, Christensen (1996) examined several cases of buckling of a flattened slab with a configuration similar to Fig. 12b.

Figures 12d, 12e and 12f show the tomographic images of the subducted slab of the Pacific plate across the southern Kurile, central Kurile arcs (Gorbatov et al., 2000) and the image of the subducted slab of the Nazca plate across Peru (Obayashi et al., 2006). The image across southern Kurile (Fig. 12d) is very similar to that across northern Bonin (Fig. 3) and may be compared to the model slab in **Fig. 12a**. The image across central Kurile (Fig. 12e) may be compared to the model slab in **Fig. 12b**. The image across Peru may be compared to the model slab in **Fig. 12c**. Although these model slabs are by no means unique, they demonstrate that slab stagnation with varied configuration is a physically feasible process to occur above, across or below the 660 discontinuity, where physical properties and thermo-mechanical states may vary to subtle extents laterally along subducting slabs and the surrounding mantle.

The stagnant slab has also been identified in the transition zone beneath North America. **Figure 13a** shows the tomographic image of the stagnant slab which is detached to the west from the Earth's surface but continues to the east down to the mid lower mantle. Schmid et al. (2002) interpreted this slab image in terms of the subduction history of the Farallon plate, as illustrated in **Fig. 13b**. The history involves slab penetration into the lower mantle, stagnation above the 660 with severe internal deformation and detachment from the surface by ridge subduction

30Ma ago. Fluid dynamic simulation by Christensen (1996) suggests that the subducted slab once stagnant above the 660 can sink into the deep lower mantle from its leading edge at a subsequent stage, if the Clapeyron slope is large enough and if trench retreat is allowed,

6. Slab falling through the lower mantle

Stagnant slab is a temporary feature and is likely to fall eventually well into the lower mantle as 'slab avalanche'. Slab avalanche may be responsible for the development of transient intracratonic basins adjacent to convergence zones (Pysklywec and Mitrovica, 1998) and the tectonic plate reorganization (Fukao et al., 2001; Pysklywec et al., 2003). Pysklywec and Ishii (2005) made an extensive numerical simulation for the effect of 'avalanche' of stagnant slabs on subduction dynamics. **Figures 14a, 14b and 14c** show an example of their results, where the stagnant slab above the 660 is detached with a large gap from the subducting slab at shallow depths. The left-top cross-section of **Fig. 14** shows the tomographic image beneath the Bering Sea across the Aleutian arc (Gorbatov et al., 2000), which is apparently analogous to the model situation at *t=0*, where the stagnant slab denser than the surrounding mantle is placed above the 660 across which there is a viscosity jump of a factor of 20 (Fig. 14a). Viscous flow coupled to the slab avalanche shifts and deforms the buoyant island arc. It also causes thinning and shearing of the downgoing slab, which eventually detaches and descending into the lower mantle (Fig.14b). Migration of the island arc makes the existing subduction zone inactive and creates a new subduction zone with reversed polarity on the back-arc side. The reversed subduction is enhanced greatly by the negative buoyancy of the newly subducted limb (Fig. 14c). This simulation implies that avalanche of a stagnant slab can trigger a reorganization of plate motion such as the one that probably occurred at the New Hebrides plate boundary at 10 Ma (Pysklywec et al., 2003). Fukao et al. (2001) argued that a synchronized fall of stagnant slabs along the circum Pacific might

have been a cause for the Eocene plate reorganization (Rona and Richardson, 1978; Gordon and Jurdy, 1986).

If the slab behavior near the 660 is complex as such, the oceanic crustal part of a slab may configure differently from the rest. It would be difficult, however, to detect such crustal part within a deeply seated slab by any conventional tomography. Alternatively, reflection analyses of seismic waves from deep shocks have been used to detect seismic reflectors or scatterers at the top of the lower mantle beneath subduction zones, which have been often attributed to fragments of subducted oceanic crust (Kaneshina and Helffrich, 2003; Kaneshima, 2003; Niu et al., 2003). **Figures 15a and 15b** show the E-W cross-sections the S wave tomographic image of the subducted slab across the northern Marian arc by Widiyantoro et al. (2000) and the P wave tomographic image across the mid Mariana arc by Fukao et al. (2001), respectively. In Fig. 15a, the seismic reflector detected and interpreted as former oceanic crust by Niu et al. (2003) is located at the bottom of the slab in the uppermost lower mantle, where they suggested that subducted crust might start sinking separately from the rest of the slab. Such crust separation is in fact a likely process in view of the recent high pressure and high temperature experiments. In Fig. 15b the seismic scatterers detected by Krüger et al. (2001) and Kaneshima (2003) are located within the severely deformed slab indented into the lower mantle. Kaneshima (2003) interpreted these scatterers as fragments of former oceanic crust entrained in the slab upon separation of crustal component from the stagnant slab near the 660 (van Keken et al., 1996; Karato, 1997). The slab images across the Mariana arc in Figs. 14a and 14b may be compared to the model slab in either **Fig. 15c** or **15d**, where there is a viscosity increase of a factor of 10 or 30, respectively, across the 660 with a Clapeyron slope of -3 MPa/K (Tagawa, 2007). No trench retreat is allowed. In this experiment (Tagawa, 2007), the model slab below the 660 is pressed flat by its indentation into the more viscous lower mantle. Seismic scatterers interpreted as the fragments of subducted oceanic crust

have been reported even at greater depths down to 2000 km (Kaneshima and Helffrich, 1999). These deep scatterers are well separated from the stagnant slab images at shallower depths. We note that descent of the oceanic crust could happen even if it is thermally in equilibrium with the surrounding lower mantle, because MORB crust is known to be denser than the normal lower mantle, as explained below.

Previous high pressure studies suggested that MORB (mid-oceanic ridge basalt) crust is buoyant at depths between 660 and 720 km (Irifune and Ringwood, 1993; Hirose et al., 1999; Litasov et al., 2004), although the situation may change if it is hydrous (Litasov et al., 2006; see Fig.10). Hirose et al. (2005) investigated phase relations, mineral chemistry and density of MORB composition to show that the post-perovskite transition (Murakami et al., 2004; Tsuchiya et al., 2004; Oganov and Ono, 2004) of MORB composition starts at a pressure lower than the transition pressure for pure MgSiO3 perovskite and ends at that pressure so that former MORB crust is denser than the average lower mantle at all depths greater than about 720 km, including the D" layer. **Figure 16** shows a comparison of the density profile of MORB composition with the reference Earth model PREM (Dziewonski and Anderson, 1981) in the whole pressure range of the lower mantle. The density profiles along the 300 and 2000K isotherms indicate that the crustal part of the subducted slab remains denser than the surrounding lower mantle even if it is thermally assimilated to the surrounding lower mantle so that it may eventually accumulate in the D" layer to differentiate its chemical nature from the rest of the mantle. Hirose et al. (1999), Ono et al. (2001, 2005) and Perrillat et al. (2006) showed that the subducted MORB crust is denser than the surrounding lower mantle although the pressure ranges they covered were limited to the shallower parts of the lower mantle. Effects of the segregation of subducted oceanic crust on isotopic fractionations in the convecting mantle have been discussed by Christensen and Hofmann (1994), Christensen (2001), Davies (2002) and

Brundenburg and van Keken (2007).

Tomographic models show some slab remnants now falling through the lower mantle (see Fukao et al. (2001) for the earlier references on this subject), the most typical examples being those of the Farallon plate and Indian (Tethys) plate. The tomographic maps in the Mediterranean region to the east of 20°E (Fig. 8; Schmid et al.; 2006) show the slab remnant of the Tethyan lithosphere whose decent initiated Late Cretaceous and now reaches a depth of at least 1500 km (Faccenna et al., 2003). The seismic signature of this remnant slab now falling through the lower mantle is characterized by positive P velocity anomaly, stronger S velocity anomaly and much weaker bulk sound velocity anomaly. According to Schmid et al. (2006), the value of $R(=[dVs/Vs]/[dVp/Vp]$ is around *1.8* in the uppermost 1000 km and appears to increase to about 2.2 below 1200 km. These values of R are in good agreement with those predicted from the mineral physics data assuming that the anomalies are due solely to temperature perturbation (Tranpart et al., 2001). The Vp, Vs and bulk sound velocity anomalies of the remnant slab of the Tethyan lithosphere in the lower mantle can be consistently interpreted as of thermal origin, for which it would be unnecessary to introduce other causes, such as compositional anomaly.

A slab falling through the lower mantle may eventually reach the core-mantle to pile up on it. It remains uncertain whether or not the deepest slab images can be interpreted solely by temperature anomalies. In Fig. 1 the stagnant slab image behind the Bonin trench is underlain by a huge body of seismically fast anomalies at the base of the mantle underneath the northwestern Pacific to eastern Asia. **Figure 16a** (Romanowicz, 2003) demonstrates that this is the largest body of fast anomalies in the lowermost mantle in almost all the existing global P tomographic models. This anomalous body develops right under the stagnant slab of the Pacific plate (Fig. 1), and may represent an ultimate graveyard of avalanche slabs in the northwestern Pacific. There

are no significant fast anomalies at depths between this graveyard image in the lowermost mantle and the stagnant slab image in the transition zone (Fig. 1), suggesting that most of the avalanche slabs in the northwestern Pacific already reached the core-mantle boundary while the present-day subducting slabs are still being accumulated in the transition zone.

This anomalous body extends northeastward geographically to northwestern Russia, where Thomas et al. (2004) detected two seismic discontinuities in the lowermost mantle by a migration study of ScS precursors. The upper discontinuity shows strong topography with a positive impedance contrast whereas the lower discontinuity exhibits much less topography with a negative impedance contrast. Thomas et al. (2004) interpreted these two discontinues as the upper and lower surfaces of the cold body of the remnant slab of the ancient Izanagi plate now trapped in the D" layer, although other interpretations may also be possible.

Figure 16b shows the perturbation maps of shear velocity, bulk sound velocity and compressional velocity at the base of the mantle in model SB10L18 by Masters et al. (2000). The compressional velocity map again indicates significant positive anomalies in the western Pacific to east China, which we interpret as the deepest slab remnants, the contemporary counterpart of which is the stagnant slabs in the transition zone (Fig. 1). The shear velocity and bulk sound velocity maps in Fig. 16b show stronger and weaker positive anomalies, respectively, in the corresponding region, where there is no anticorrelation between shear velocity anomaly and bulk sound velocity anomaly such as the one observed in the central Pacific. At present, there is little evidence that the slab remnants in the lowermost mantle under the western Pacific and east China are chemically anomalous.

7. Summary

Collaboration of seismic and electromagnetic observations,

mineral physics measurements, and geodynamic modeling begins to provide a consistent picture of stagnant slab. The review presented here may be summarized as follows.

(1)Stagnant slab is a phenomenon commonly observed beneath subduction zones around the circum Pacific and in the Mediterranean at depths above, across or below the 660.

(2)The “seismological” Clapeyron slope of the 660 is negatively greater than the recent experimental values for decomposition of dry ringwoodite. This observation seems to suggest that the ringwoodite regime under a subduction zone is hydrated. There is little evidence, however, that the stagnant slab is more hydrated than the surrounding transition zone.

(3)Numerous fluid-dynamic simulations of plate subduction indicate that stagnant slab with varied configuration is a geodynamically feasible process to occur in some depth range above, across or below the 660.

(4)The heavier crustal component may be detached from a stagnant slab upon its severe distortion to sink separately through the lower mantle.

(5)There is growing evidence that geophysical signatures, including P, S and bulk sound velocities and electrical conductivity, of both stagnant slabs in the transition region and falling slabs in the lower mantle are primarily of thermal origin, compositionally little different from the surrounding mantle.

References

Akaogi, M., and E. Ito (1993), Refinement of enthalpy measurement of MgSiO3 perovskite and negative pressure-temperature slopes for perovskite-forming reactions, Geophys. Res. Lett., 20, 1839-1842.

Bijwaard H., W. Spakman, E.R. Engdahl (1998), Closing the gap between regional and global travel time tomography, J. Geophys. Res. 103, 30055-30078.

Bina, C. R., and G. R. Helffrich (1994), Phase transition Clapeyron slopes and transition zone seismic discontinuity topography, J. Geophys. Res., 99, 15,853-15,860.

Bolfan-Casanova, N. (2005), Water in the Earth's mantle, Mineral. Magazine, 69, 229-257.

Bolton, H., and G. Masters (2001), Travel times of P and S from the global digital networks: implications for the relative variation of P and S in the mantle. J. Geophys. Res., 106, 13,527-13,540.

Brandenburg, J.P., and P.E. van Keken, (2007), Deep storage of oceanic crust in a vigorously convecting mantle, J. Geophys. Res., 112, B06403.

Cammarano, F., S. Goes, P. Vacher, and D. Girdini (2003), Inferring upper-mantle temperatures from seismic velocities, Phys. Earth Planet. Inter., 138, 197-222.

Christensen, U.R. (1996), The influence of trench migration on slab penetration into the lower mantle, Earth Planet. Sci. Lett, 140, 27-39.

Christensen, U.R. (2001), Geodynamic models of deep subduction, Phys. Earth Planet. Int., 127, 25-34.

Christensen, U. R. and D. A. Yuen (1995), Layered convection induced by phase transitions, J. Geophys. Res., 90, 10291-10300.

Christensen, U.R., and A.W. Hofmann (1994), Segregation of subducted oceanic crust in the convecting mantle, J. Geophys. Res., 99, 19867-19884.

Čížková, H., J. van Hunen, A.P. van den Berg, and N.J. Vlaar (2002), The influence of rheological weakening and yield stress on the interaction of slabs with the 670 km discontinuity, Earth Planet. Sci. Lett., 199, 447-457.

Davies, G.F. (2002), Stirring geochemistry in mantle convection models with stiff plates and slabs, Geochim. Cosmochim. Acta, 66, 3125-3142.

Deschamps, F., and J. Trampert (2003), Mantle tomography and its relation to temperature and composition, Phys. Earth Planet. Inter., 140, 277-291.

Dziewonski, A., and D. L. Anderson (1981), Preliminary reference Earth model. Phys. Earth Planet. Inter. 25, 297-356.

Engdahl, E., R. van der Hilst, and R. Buland (1998), Global teleseismic earthquake relocation with improved travel times and procedures for depth determination, Bull. Seismol. Soc. Am., 88, 722-743.

Faccenna, C., L. Jolivet, C. Piromallo, and A. Morelli (2003), Subduction and the depth of convection in the Mediterranean mantle, J. Geophys. Res., 108, B2, 2099, doi:10.1029.

Fei, Y., J. Van Orman, J. Li, W. van Westrenen, C. Sanloup, W. Minarik, K. Hirose, T. Komabayashi, M. Walter, and K. Funakoshi (2004), Experimentally determined postspinel

transformation boundary in Mg2SiO4 using MgO as an internal pressure standard and its geophysical implications, J. Geophys. Res., 109, B02305, doi:10.1029/2003JB002562.

Flanagan, M. P., and P. M. Shearer (1998), Global mapping of topography on transition zone velocity discontinuity by stacking SS precursors, J. Geophys. Res., 103, 2673-2692.

Forte, A.M., A.M. Dziewonski, and R.L. Woodward (1993), Aspherical structure of the mantle, tectonic plate motions, nonhydrostatic geoid, and topography of the core-mantle boundary, in Dynamics of the Earth's Deep Interior and Earth Rotation, AGU Geophysical Monograph, 72, 135-166.

Friederich, W. (2003), The S-velocity structure of the East Asian mantle from inversion of shear and surface waveforms, Geophys. J. Int., 153, 88-102.

Fukao, Y., T. Koyama, M. Obayashi, and H. Utada (2004), Trans-Pacific temperature field in the mantle transition region derived from seismic and electromagnetic tomography, Earth Planet. Sci. Lett., 217, 425-434.

Fukao, Y., M. Obayashi, H. Inoue, and M. Nenbai (1992), Subducting slabs stagnant in the mantle transition zone, J. Geophys. Res., 97, 4809-4822.

Fukao, Y., S. Widiyantoro, and M. Obayashi (2001), Stagnant slabs in the upper and lower mantle transition region, Rev. Geophys., 39, 291-323.

Gorbatov, A., S. Widiyantoro, Y. Fukao, and E. Gordeev (2000), Signature of remnant slabs in the North Pacific from P-wave tomography, Geophys. J. Int., 142, 27-36.

Gorbatov, A., B. L. N. Kennett (2002), Joint bulk-sound and shear

tomography for western Pacific subduction zones. Earth Planet Sci Lett 210, 527-543.

Gorbatov, A. and Y. Fukao (2005), Tomographic search for missing link between the remnant Farallon slab and present Cocos subduction, Geophys. J. Int., 160, 849-854.

Gordon, R.G., and D.M. Jurdy (1986), Cenozoic global plate motions, J. Geophys. Res., 91, 12389-12406.

Grand, S.P. (1994), Mantle shear structure beneath the Americas and surrounding oceans, J. Geophys. Res., 99, 11591-11621.

Grand, S.P. (2002), Mantle shear-wave tomography and the fate of subducted slabs, Phil. Trans. R. Soc. Lond. A, 360, 2475-2491.

Grand, S., R. van der Hilst, S. Widiyantoro, (1997), Global seismic tomography: a snapshot of convection in the Earth. GSA Today 7, 1-7.

Gu, Y.J., A. Dziewonski, and G. Ekström (2003), Simultaneous inversion for mantle shear velocity and topography of transition discontinuities, Geophys. J. Int., 154, 559-583.

Gurnis, M., and B. H. Hager (1988), Controls on the structure of subducted slabs, Nature, 335, 317-322.

Hafkenscheid, E., M.J.R. Wortel, and W. Spakman (2006), Subduction history of the Tethyan region derived from seismic tomography and tectonic reconstructions, J. Geophys. Res., 111, B08401.

Higo, Y., T. Inoue, and T. Irifune (2001), Effect of water on the spinel-postspinel transformation in Mg2SiO4, Geophys. Res. Lett., 28, 3505-3508.

Higo,Y., T. Inoue, T. Irifune, K. Funakoshi and B. Li (2007), Elastic wave velocities of (Mg0.91Fe0.09)2SiO4 ringwoodite under P-T conditions of the mantle transition region (submitted to PEPI, July 2007).

Hirose, K., Fei, Y., Ma, Y., and Mao, H.K. (1999), The fate of subducted basaltic crust in the Earth's lower mantle. Nature 397, 53-56.

Hirose, K., N. Takafuji, N. Sata, and Y. Ohishi (2005), Phase transition and density of subducted MORB crust in the lower mantle, Earth Planet. Sci. Lett., 237, 239-251.

Hirose, K., N. Takafuji, N. Sata, and Y. Ohishi (2005), Phase transition and density of subducted MORB crust in the lower mantle, Earth Planet. Sci. Lett., 237, 239-251.

Honda, S., D. A. Yuen, S. Balachandar, and D. Reuteler (1993), Three-dimensional instabilities of mantle convection with multiple phase transitions, Science, 259. 1308 – 1311.

Huang, X., X. Yousheng, and S. Karato (2005), Water content in the transition zone from electrical conductivity of wadsleyite and ringwoodite, 434, 746-749.

Huang, J., and D. Zhao (2006), High-resolution mantle tomography of China and surrounding regions, J. Geophys. Res., 111, B09305.

Ichiki, M., K. Baba, M. Obayashi and H. Utada (2006), Water content and geotherm in the upper mantle above the stagnant slab: Interpretation of electrical conductivity and seismic P-wave velocity models, Phys. Earth Planet. Inter., 155, 1-15.

Inoue, T., H. Yurimoto and Y. Kudoh (1995), Hydrous modified spinel, $Mg_{1.75}SiH_{0.5}O_4$: a new water reservoir in the mantle

transition region, Geophys. Res. Lett., 22, 117-120.

Inoue, T., D. J. Weidner, P. A. Northrup and J. B. Parise (1998), Elastic properties of hydrous ringwoodite (γ-phase) on Mg_2SiO_4, Earth Planet. Sci. Lett., 160, 107-113.

Irifune, T., and A. E. Ringwood (1993), Phase transformations in subducted oceanic crust and buoyancy relationships at depths of 600-800 km in the mantle, Earth Planet. Sci. Lett. 117, 101-110.

Irifune, T., N. Nishiyama, K. Kuroda, T. Inoue, M. Isshiki, W. Utsumi, K. Funakoshi, S. Urakawa, T. Uchida, T. Katsura, and O. Ohtaka (1998), The postspinel phase boundary in Mg2SiO4 determined by in situ X-ray diffraction, Science, 279, 1698-1700.

Irifune, T., Y. Higo, T. Inoue, Y. Kono, K. Funakoshi (2007), Sound velocities of majorite garnet and the composition of the mantle transition region (submitted to Nature).

Ito, E., and E. Takahashi (1989), Post-spinel transformation in the system Mg2SiO4-Fe2SiO4 and some geophysical implications, J. Geophys. Res., 94, 10,637-10,646.

Ito, E. and H. Sato (1991), Aseismicity in the lower mantle by superplasticity of the descending slab, Nature, 351, 140-141.

Jacobsen, S. D., J. R. Smyth, H. Spetzler, C. M. Holl, and D. J. Frost (2004), Sound velocity and elastic constants of iron-bearing hydrous ringwoodite, Phys. Earth Planet. Inter., 143-144, 47-56.

Jacobsen, S.D., and J.R. Smyth (2006), Effect of water on the sound velocities of ringwoodite in the transition zone, in Earth's Deep Water Cycle, AGU Geophysical Monograph, 167, 131-145.

Kaneshima, S. (2003), Small-scale heterogeneity at the top of the lower mantle around the Mariana slab, Earth Planet. Sci. Lett.,

209, 85-101.

Kaneshima, S., and G. Helffrich (1999), Dipping low-velocity layer in the midlower mantle: Evidence for geochemical heterogeneity, Science, 283, 1888-1891.

Kaneshima, S., and G. Helffrich (2003), Subparallel dipping heterogeneities in the mid-lower mantle, J. Geophys. Res., 108, doi:10.1029/2001JB001596.

Katsura, T., H. Yamada, T. Shinmei, A. Kubo, S. Ono, M. Kanzaki, A. Yoneda, M. J. Walter, E. Ito, S. Urakawa, K. Funakoshi, W. Utsumi (2003), Post-spinel transition in Mg2SiO4 determined by high P-T in situ X-ray diffractometry, Phys. Earth Planet. Inter., 136, 11-24.

Karato, S. (1997), On the separation of crustal component from subducted oceanic lithosphere near the 660 km discontinuity, Phys. Earth Planet. Int., 99, 103-111.

Karato, S., D. Bercovici, G.Leathy, G. Richard, and Z. Jing (2006), The transition-zone water filter model for global material circulation: Where do we stand?, in Earth's Deep Water Cycle, AGU Geophysical Monograph, 167, 289-313.

Karato, S., and P. Wu (1993), Rheology of the upper mantle: A synthesis, Science, 260, 771-778.

Kawakatsu H., and S. Watada (2007), Seismic evidence for deep water transportation in the mantle, Science, 316, 1468-1471.

Kennett, B., and E. Engdahl (1991), Traveltimes for global earthquake location and phase identification. Geophys. J. Int. 105, 429-465.

Kennett, B.L.N., and A. Gorbatov (2004), Seismic heterogeneity in

the mantle – strong shear wave signature of slabs from joint tomography, Phys. Earth Planet. Inter., 146, 87-100.

Kohlstedt, D. L., H. Keppler, D. C. Rubie (1996), Solubility of water in the α, ß, and γ phases of $(Mg, Fe)_2SiO_4$. Contrib. Miner. Petrol., 123, 345-357.

Komabayashi, T., and S. Omori, (2006), Internally consistent thermodynamic data set for dense hydrous magnesium silicate up to 35 GPa, 1600^o C: Implications for water circulation in the Earth's deep mantle, Phys. Earth Planet. Int., 156, 89-107.

Koyama, T., H. Shimizu, H. Utada, M. Ichiki, E. Ohtani, and R. Hae (2006), Water Content in the Mantle Transition Zone Beneath the North Pacific Derived From the Electrical Conductivity Anomaly, AGU Geophys. Monogr. Ser., 168, 171-179, .

Krüger, F., M. Baumann, F. Scherbaum, and M. Weber (2001), Mid mantle scatterers near the Mariana slab detected with a double array method, Geophys. Res. Lett., 28, 667-670.

Lei, J., and D. Zhao (2005), P-wave tomography and origin of the Changbai intraplate volcano in Northeast Asia, Tectonophysics, 397, 281-295.

Lei, J., D. Zhao (2006) Global P-wave tomography: on the effect of various mantle and core phases. Phys. Earth Planet. Inter. 154, 44-69.

Levedev, S., S. Chevrot, and R. D. van der Hildt (2002), Seismic evidence for olivine phase changes at the 410- and 660-kilometer discontinuities, Science, 296, 1300-1302.

Li, X. D, and B. Romanowicz (1996), Global mantle shear velocity model using nonlinear asymptotic coupling theory, J. Geophys.

Res., 101, 22,245-22,272.

Li, L., D.J. Weidner, J. Brodholt, D. Alfè (2006), Elasticity of Mg2SiO4 ringwoodite at mantle conditions, Phys. Earth Planet. Inter., 157, 181-187.

Li, X, and X. Yuan (2003), Recwiver functions in northeast China – implications for slab penetration into the lower mantle in northwest Pacific subduction zone, Earth Planet. Sci. Lett., 216, 679-691.

Litasov, K., E. Ohtani, A. Suzuki, T. Kawazoe, and K. Funakoshi (2004), Absence of density crossover between basalt and peridotite in the cold slabs passing through 660 km discontinuity, Geophys. Res. Lett., 31, L24607, doi:10.1029/2004GL021306.

Litasov, K. D., E. Ohtani, A. Sano, and A. Suzuki (2005), Wet subduction versus cold subduction, Geophys. Res. Lett., 32, doi:10.1029/2005GL022921.

Litasov, K., E. Ohtani, A. Sano, A. Suzuki, and K. Funakoshi (2005), In situ X-ray diffraction study of post-spinel transformation in a peridotite mantle: Implication for the 660-km discontinuity, Earth Planet. Sci. Lett., 238, 311-328.

Litasov, K.D., E. Ohtani, and A. Sano (2006), Influence of water on major phase transitions in the Earth's mantle, in Earth's Deep Water Cycle, AGU Geophysical Monograph, 167, 95-111.

Machetel, P. and P. Weber (1991), Intermittent layered convection in a model mantle with an endothermic phase change at 670 km, Nature, 350, 55-57.

Marone, F., van der Lee, S., Giardini, D., 2004. Three-dimensional upper-mantle S-velocity model for the Eurasia-Africa plate boundary region. Geophys. J. Int. 158, 109-130.

Masters, G., G. Laske, H. Bolton, and A. Dziewonski (2000), The relative behavior of shear velocity, bulk sound speed, and compressional velocity in the mantle: implications for chemical and thermal structure, in: Earth's deep interior, AGU Monograph 117, Ed S. Karato, 63—87.

Mitrovica, J. X., and A. M. Forte (1997), Radial profile of mantle viscosity: Results from the joint inversion of convection and postglacial rebound observables, J. Geophys. Res., 2751-2770.

Mayama, M., I. Suzuki, T. Saito, I. Ohno, T. Katsura, and A. Yoneda (2005), Temperature dependence of the elastic moduli of ringwoodite, Phys. Earth Planet. Inter., 148, 353-359.

Murakami, M., K. Hirose, K. Kawamura, N. Sata, and Y. Ohishi (2004), Post-perovskite phase transition in MgSiO3, Science, 304, 855-858.

Nishihara, Y., T. Shinmei, and S. Karato (2006), Grain-growth kinetics in wadsleyite: Effects of chemical environment, Phys. Earth Planet. Int., 154, 30-43.

Niu, F., H.Kwakatsu and Y.Fukao (2003), Seismic evidence for a chemical heterogeneity in the midmantle: A slightly dipping and strong seismic reflector at mid-depth beneath the Mariana subduction zone, J. Geophys. Res., 108, JB002384.

Niu, F., A. Levander, S. Ham, and M. Obayashi (2005), Mapping the subducting Pacific slab beneath southwest Japan with Hi-net receiver functions, Earth Planet. Sci. Lett., 239, 9-17.

Obayashi M., H. Sugioka, J. Yoshimitsu, Y. Fukao (2006), High temperature anomalies oceanward of subducting slabs at the 410-km discontinuity, Earth Planet. Sci. Lett., 243, 149-158.

Oganov, A. R., and S. Ono (2004), Theoretical and experimental evidence for a post-perovskite phase of MgSiO3 in Earth's D”layer, Nature, 430, 445-448.

Ohtani, E., K. Litasov, T. Hosoya, T. Kubo, and T. Kondo (2004), Water transport into the deep mantle and formation of a hydrous transition zone, Phys. Earth Planet. Inter., 143-144, 255-269.

Okino, K., M., Ando, S. Kaneshima, and K. Hirahara (1989), The horizontally lying slab, Geophys. Res. Lett., 16, 1059-2062.

Ono, S., Ito, E., and Katsura, T. (2001), Mineralogy of subducted basaltic crust (MORB) from 25 to 37 GPa, and chemical heterogeneity of the lower mantle. Earth Planet. Sci. Lett. 190, 57-63.

Ono, S., Ohishi, Y., Isshiki, M., and Watanuki, T. (2005), In situ Xray observations of phase assemblages in peridotite and basalt compositions at lower mantle conditions: implications for density of subducted oceanic plate. J. Geophys. Res. 110 (B02208), doi:10.1029/2004JB003196.

Perrillat, J.-P., A. Ricolleau, I. Daniel, G. Fiquet, M. Mezouar, N. Guignot, and H. Cardon (2006), Phase transformations of subducted basaltic crust in the upmost lower mantle, Phys. Earth Planet. Int., 157, 139-149.

Piromallo, Claudia, and A. Morelli (2003), P wave tomography of the mantle under the Alpine-Mediterranean area, J. Geophys. Res., 108, B2, 2065.

Pysklywec, R., and J. X. Mitrovica (1998), Mantle Flow Mechanisms for the Large-Scale Subsidence of Continental Interiors, Geology, 26, 687-690.

Pysklywec, R. N., J. X. Mitrovica, and M. Ishii (2003), Mantle

avalanche as a driving force for tectonic reorganization in the southwest Pacific, Earth Planet. Sci. Lett., 209, 29-38.

Pysklywec, R.N., and M. Ishii, (2005), Time dependent subduction dynamics driven by the instability of stagnant slabs in the transition zone, Phys. Earth Planet. Inter., 149, 115-132.

Replumaz, A., H. Kárason, R.D. van der Hilst, J. Besse, and P. Tapponnier, 4-D evolution of SE Asia's mantle from geological reconstructions and seismic tomography (2004), Earth Planet. Sci. Lett., 221, 103-115.

Richard, G., D. Bercovici, and S. Karato (2006), Slab dehydration in the Earth's mantle transition zone, Earth Planet. Sci. Lett., 251, 156-167.

Richard, G., M. Monnereau, and M. Rabinowicz (2007), Slab dehydration and fluid migration at the base of the upper mantle: implications for deep earthquake mechanisms, Geophys. J. Int., 168, 1291-1304.

Riedel, M.R., and S. Karato (1997), Grain-size evolution in subducted oceanic lithosphere associated with the olivine-spinel transformation and its effects on rheology, Earth and Planet. Lett., 148, 27-43.

Romanowicz, B. (2003), Global mantle tomography: Progress status in the past 10 years, Annu. Rev. Earth Planet. Sci., 31, 303-328.

Rona, P.A., and E.S. Richardson (1978), Early Cenozoic global plate reorganization, Earth Planet. Sci. Lett., 40, 1-11.

Rubie, D. C. (1984), The olivine!spinel transformation and the rheology of subducting lithosphere, Nature, 308, 505-508.

Schubert, G., and G.L. Turcotte (1971), Phase changes and mantle convection, J. Geophys. Res., 76, 1424-1432.

Schmid, C., S. Goes, S. van der Lee, and D. Giardini (2002), Fate of the Cenozoic Farallon slab from a comparison of kinematic thermal modeling with tomographic images, Earth and Planet. Lett., 2002, 17-32.

Schmid, C., S. van der Lee, and D. Giardini (2006), Correlated shear and bulk moduli to 1400 km beneath the Mediterranean region, Phys. Earth Planet. Int., 159, 213-224.

Sinogeikin, S.V., Bass, J.D., and Katsura, T. (2001), Single-crystal elasticity of -$(Mg_{0.91}Fe_{0.09})_2SiO_4$ to high pressures and to high temperatures. Geophys. Res. Lett. 28, 4335-4338.

Sinogeikin, S.V., J. D. Bass, and T. Katsura (2003), Single-crystal elasticity of ringwoodite to high pressures and high temperatures: implications for 520 km seismic discontinuity, Phys. Earth Plane. Inter., 136, 41-66.

Solheim, L.P., and W.P. Peltier, Avalanche effects in phase transition modulated thermal convection: a model of Earth's mantle (1994), J. Geophys. Res., 99, 6997-7018.

Su, W., R. L. Woodward, and A. M. Dziewonski (1994), Degree 12 model of shear velocity heterogeneity in the mantle, J. Geophys. Res., 99, 6945-6980.

Suetsugu, D., T. Inoue, A. Yamada, D. Zhao, and M. Obayashi (2006), Towards Mapping the three-dimensional distribution of water in the transition zone from P-velocity tomography and 660-km discontinuity depths, in Earth's Deep Water Cycle, AGU Geophysical Monograph, 167, 237-249.

Sugioka, H., D. Suetsugu, M. Obayashi, Y. Fukao, and Y. Gao (2007), Body wave travel time anomalies associated with the stagnant slab (abstract), IUGG 2007, JSS012.

Tackley, P. J., D. J. Stevenson, G. A. Glatzmaier, and G. Schubert (1993), Effects of an endothermic phase transition at 670 km depth in a spherical model of convection in the Earth's mantle, Nature, 361, 699-704.

Tagawa, M. (2007), Numerical modeling of slab dynamics: history-dependent rheology and slab stagnation mechanisms, Doctor Thesis, pp. 218, Hiroshima University.

Tagawa, M., T. Nakakuki, and F. Tajima (2007), Dynamical modeling of trench retreat driven by the slab interaction with the mantle transition zone, Earth Planets Space, 59, 65-74.

Tarits, P., S. Hautot, and F. Perrier (2004), Water in the mantle: Results from electrical conductivity beneath the French Alps, Geophys. Res. Lett., 31, L06612.

Tetzlaff, M. and H. Schmeling (2000), The influence of olivine metastability on deep subduction of oceanic lithosphere, Phys. Earth Planet. Int.,120, 29-38.

Thomas, C., J-M. Kendall, and J. Lowman (2004), Lower-mantle seismic discontinuities and the thermal morphology of subducted slabs, Earth Planet. Sci. Lett., 225, 105-113.

Tono, Y., T. Kunugi, Y. Fukao, S. Tsuboi, K. Kanjo, and K. Kasahara (2005), Mapping of the 410- and 660-km discontinuities beneath the Japanese islands, J. Geophys. Res., 110, doi:10.1029/2004JB003266.

Torii, Y., and S. Yoshioka (2007), Physical conditions for slab stagnation: Cnstraints from Clapeyron slope, mantle viscosity,

trench retreat, and dip angles, Tectonophysics (in press).

Trampert, J., P. Vacher, and N. Vlaar (2001), Sensitivities of seismic velocities to temperature, pressure and composition in the lower mantle, Phys. Earth Planet. Int., 124, 255-267.

Tsuchiya, T., J. Tsuchiya, K. Umemoto and R. M. Wentzcovitch (2004), Elasticity of post-perovskite MgSiO3, Geophys. Res. Lett., 31, L14603 doi:10.1029/2004GL020278.

Utada, H., T. Koyama, M. Obayashi, and Y. Fukao (2007), Electrical conductivity in the mantle transition region beneath Europe, (Nature, submitted).

van der Hilst, R.D., E.R. Engdahl, W. Spakman, and G. Nolet (1991), Tomographic imaging of subducted lithosphere below northwest Pacific island arcs, Nature, 353, 37-43.

van der Hilst, R.D., E.R. Engdahl, and W. Spakman (1993), Tomographic inversion of P and pP data for aspherical mantle structure below the northwest Pacific region, Geophys. J. Int., 115, 264-302.

van der Hilst, R., S. Widiyantoro, and E. Engdahl (1997), Evidence for deep mantle circulation from global tomography. Nature 386, 578-584.

Van der Lee, S. and G. Nolet (1997), Seismic image of the subducted trailing fragments of the Farallon plate, Nature, 386, 266-269.

van der Meijde, S. van der Lee, and D. Giardini (2005), Seismic discontinuities in the Mediterranean mantle, 148, 233-250.

van der Voo, R., W. Spakman, and H. Bijwaard (1999), Mesozoic subducted slabs under Siberia, Nature, 397, 246-249.

van Keken, P.E., S. Karato, and D.A. Yuen (1996), Rheological control of oceanic crust separation in the transition zone, Geophys. Res. Lett., 23, 1821-1824.

Wang, D., M. Mookgerjee, Y. Xu, and S. Karato (2006), The effect of water on the electrical conductivity of olivine, Nature, 443, 977-980.

Wang, J., S. V. Sinogeikin, T. Inoue and J. D. Bass (2003), Elastic properties of hydrous ringwoodite, Am. Mineral., 88, 1608-1611.

Wang, J., S.V. Sinogeikin, T. Inoue, and J.D. Bass (2006), Elastic properties of hydrous ringwoodite at high-pressure conditions, Geophys. Res. Lett., 33, L14308.

Wicks, C. W., Jr., and M. A. Richards (1993), A detailed map of the 660-kilometer discontinuity beneath the Izu-Bonin subduction zone, Science, 261, 1424-1427.

Widiyantoro, S., B.L.N. Kennett, and R.D. van der Hilst (1999), Seismic tomography with P and S data reveals lateral variations in the rigidity of deep slabs, Earth Planet. Sci. Lett., 173, 91-100.

Widiyantoro, S., A. Gorbatov, B. L. N. Kennett, and Y. Fukao (2000), Improving global shear wave traveltime tomography using three-dimensional ray tracing and iterative inversion, Geophys. J. Int., 141, 747- 758.

Xu, Y., Shankland, T. J. & Poe, B. T., Laboratory-based electrical conductivity in the Earth's mantle, J. Geophys. Res. 105, 27,865-27,875, (2000).

Yamagishi. Y., T. Yanagisawa, and Y. Hamano (2004), The rhythm of the interior activity of the Earth controlled by mantle

convection, 9th Symposium Study of the Earth's Deep Interior, Kongresshaus Garmisch-Partenkirchen, Germany, July 2004.

Yamazaki, D., T. Inoue, M. Okamoto, and T. Irifune (2005), Grain growth kinetics of ringwoodite and its implication for rheology of the subducting slab, Earth Planet. Sci. Lett., 236, 871-881.

Yoshioka S., and H. Sanshadokoro (2002), Numerical simulations of deformation and dynamics of horizontally lying slabs, Geophys. J. Int., 151, 69-82.

Zhao, D. (2004), Global tomographic images of mantle plumes and subducting slabs: insight into deep Earth dynamics, Phys. Earth Planet. Inter., 146, 3-34.

Figure captions

Figure 1. A wide-angle slice of the P-wave tomographic model of the Earth's mantle (Fukao et al., 2001), showing the stagnant slab of the Pacific plate behind the Honshu arc and the probable slab remnants in the deepest lower mantle.

Figure 2. E-W vertical cross-sections of P wave velocity perturbations along latitudes 41°, 39° and 37°, where the horizontal slab (=stagnant slab) extends over a distance of 800 to 1000 km above the 660-km discontinuity (modified from Huang and Zhao (2006) with permission). Line PP' in the map is the profile for the cross-sections in Fig. 3.'The star mark in (c) is the hypocenter of a deep shock relevant to Fig. 4.

Figure 3. Vertical cross-sections of bulk sound velocity and shear velocity anomalies across the Izu-Bonin and Ryukyu arcs along profile PP' in the map of Fig. 2 (Gorbatov and Kennett, 2003). The downgoing part of the subducted slab is strongly anomalous in shear velocity but only slightly in bulk-sound velocity, while the horizontal portion is more anomalous in bulk-sound velocity than in shear velocity.

Figure 4. Vertical P and transverse S broadband seismograms at stations in southwest Japan and China for the Izu-Bonin deep shock of June 03, 2002 (Sugioka et al., 2007). See Fig. 2c for the hypocenter. The visually picked P and S arrivals are marked by red dots. The calculated arrivals for the three-dimensional (3D) P and S velocity models are indicated by open dots. The 3D P velocity model is referred to Obayashi et al. (2006), which is coveted to the 3D S velocity model using an appropriate conversion factor (see the text for the detail). The reference travel time curve is isap91 (Engdhal et al., 1998). The arrows on the left and right sides indicate the distance range where the P and S rays should be strongly affected by the stagnant slab.

Figure 5. P-wave tomographic maps of Obayashi et al. (2006) in three depth ranges, (a)just above the 410-km discontinuity, (b)in the mid transition zone and (c)around the 660-km discontinuity. Strongly fast anomalies in (a), (b) and (c) are associated with the downgoing part, flattening part and bottoming part of the subducted slab of the Pacific plate, respectively. Line AA' in (c) is the profile along which cross-sections are taken in Fig.6. The contours in (c) are the depth anomalies in km of the 660 obtained by a receiver function analysis of Lie and Yuan (2003).

Figure 6. Cross-sections across the Izu-Bonin arc along profile AA' in Fig. 5c. (a)P-wave tomographic cross-section of the subducted ,,slab image showing its downgoing part, bottoming part and flattening part which correspond to the slab images in Figs. 5a, 5c and 5b, respectively (Obayashi et al., 2006). (b)Topographic cross-section of the 660, which is marked by a lateral continuation of strong signal of S to P conversion (Niu et al., 2005). The depression of the 660 is greatest in the bottoming part of the subducted slab. Superposed is the P velocity anomaly variation at a constant depth of 660 km along the same profile. The topographic depression (scale on the left) and the positive velocity anomaly (scale on the right) are remarkably parallel to each other.

Figure 7. P- and S-velocities of ringwoodite and majorite ultrasonically measured at various pressures and temperatures corresponding 'directly' to those in the transition zone (Higo et al., 2007).

Figure 8. Tomographic maps of P, S and bulk sound velocity anomalies below south Europe, obtained by a joint inversion of P, S and Rayleigh wave data (Schmid et al., 2006). The inferred stagnant slab region is encircled by square in each of the maps at 500-km depth. Roughly to the east of 20^{o} E, the Mediterranean lithosphere appears to subduct to depths beyond 1200 km.

Figure 9. (a)Tomographic map of electrical conductivity at a depth of 500 km, obtained by an inversion of the regional geomagnetic data in Europe (Utada et al., 2007, in preparation). The map shows the spatial variation of logarithmic ratio of 3D electrical conductivity σ to its 1D reference σ_{1D}. The stagnant slab is imaged as an extensive horizontal spread of low electrical conductivity. The star mark indicates the location at which Tarits et al. (2004) estimated the underlying electrical conductivity structure. (b)Temperature anomaly distribution converted from the electrical conductivity anomaly distribution.

Figure 10. Effects of water on phase transition of olivine at pressures and temperatures corresponding to the 410-km discontinuity and phase decomposition of ringwoodite at those corresponding to the 660-km discontinuity (Litasov et al, 2006), Arrow indicates shift of the phase boundary by addition of water.

Figure 11: Three modes of convection pattern (Yamagishi et al., 2006). (a)Pattern change from the one-layered to two-layered mode through the intermittent mode. (b)Existent ranges of the three modes in the Clapeyron slope versus Rayleigh number diagram for a uniform viscosity mantle with 3D spherical shell geometry. The phase transition occurs at 660-km depth. The Rayleigh number is defined for the system component heated from below. Half of the heating comes from the system component internally heated. The ranges of "seismological" Clapeyron slope and"basal" Rayleigh number are shown by arrows along the vertical and horizontal axes, respectively.

Figure 12. Comparison of stagnant slab images between fluid-dynamic simulation and seismic tomography. Fluid-dynamic simulation allows one-sided subduction to occur along the megathrust. Trench migration is also allowed. Viscosity is strongly temperature-dependent so that the viscosity profile shown here gives a measure of the temperature profile. Softening due to grain size reduction associated with phase transition

occurs in the colder part ($T<To$) of the slab. In (a), (b) and (c), the Clapeyron slope is -2, -3 and -1 MPa/K and the critical temperature To is 1073, 1873 and 1073 K, respectively (Tagawa, 2007). The corresponding P-wave tomographic images of subducted slab are those across the southern Kurile and central Kurile arcs (Gorbatov et al., 2000) and that across Peru (Obayashi et al., 2006) in (d), (e) and (f), respectively.

Figure 13. S-wave tomographic image of the slab remnant of the Farallon plate beneath North America and its plate tectonic interpretation (Schmid et al., 2001). (a)Tomographic image synthesized from the upper mantle model of van der Lee and Nolet (1997) and the whole mantle model of Grand (1994). The remnant slab of the Farallon plate is now stagnant in the transition zone, which is detached to the west from the Earth's surface but continues to the east down to the mid lower mantle. (b)Interpretation of the slab image in terms of the subduction history of the Farallon plate. The history involves slab penetration into the lower mantle, stagnation above the 660 and detachment from the surface by ridge subduction.

Figure 14. (Left-top)P-wave tomographic image of the stagnant slab above the 660, which is detached well from the subducting slab from the Aleutian trench (Gorbatov et al., 2000). (a-c)Effect of 'avalanche' of stagnant slab on subduction dynamics (Pysklywec and Ishii, 2005). The stagnant slab above the 660 is detached with a large gap from the subducting slab at shallow depths. Across the 660 there is a viscosity jump of a factor of 20 (a). Viscous flow coupled to the slab avalanche shifts and deforms the buoyant island arc (b). Migration of the island arc makes the existing subduction zone inactive and creates a new subduction zone with reversed polarity on the back-arc side (c).

Figure 15. E-W cross-sections of the S wave tomographic image of the subducted slab across the northern Marian arc (a) and the P wave tomographic image (b) across the mid Mariana arc (b), In (a)

(Widiyantoro et al., 2000) the seismic reflector detected and interpreted as former oceanic crust is indicated by red line (Niu et al., 2003). In (b) (Fukao et al., 2001) the seismic scatterers detected by Krüger et al. (2001) and Kaneshima (2003) are indicated by small and large dots. Kaneshima (2003) interpreted these scatterers as fragments of former oceanic crust.

Figure 16. Rock density of MORB crust in the lower mantle (after Hirose et al., 2005). Closed and open symbols indicate 300 K and high temperature (1750-2290 K) data, respectively. Broken lines indicate the PREM density. The subducted MORB is denser than the surrounding mantle except between the 660-km boundary and 720-km depth. The density contrast is about 3% at the base of the mantle.

Figure 17. (a)Lowermost mantle anomalies of global P-wave tomographic models compiled by Romanowicz (2003). (b)Perturbation maps of shear velocity, bulk sound velocity and compressional velocity at the base of the mantle in model SB10L18 by Masters et al. (2000). For all the models, the northwestern Pacific to eastern China region encircled by black ellipse is commonly characterized by positive velocity anomalies, which may represent an ultimate graveyard of fallen slabs in the northwestern Pacific.

Fukao et al. Figure 1

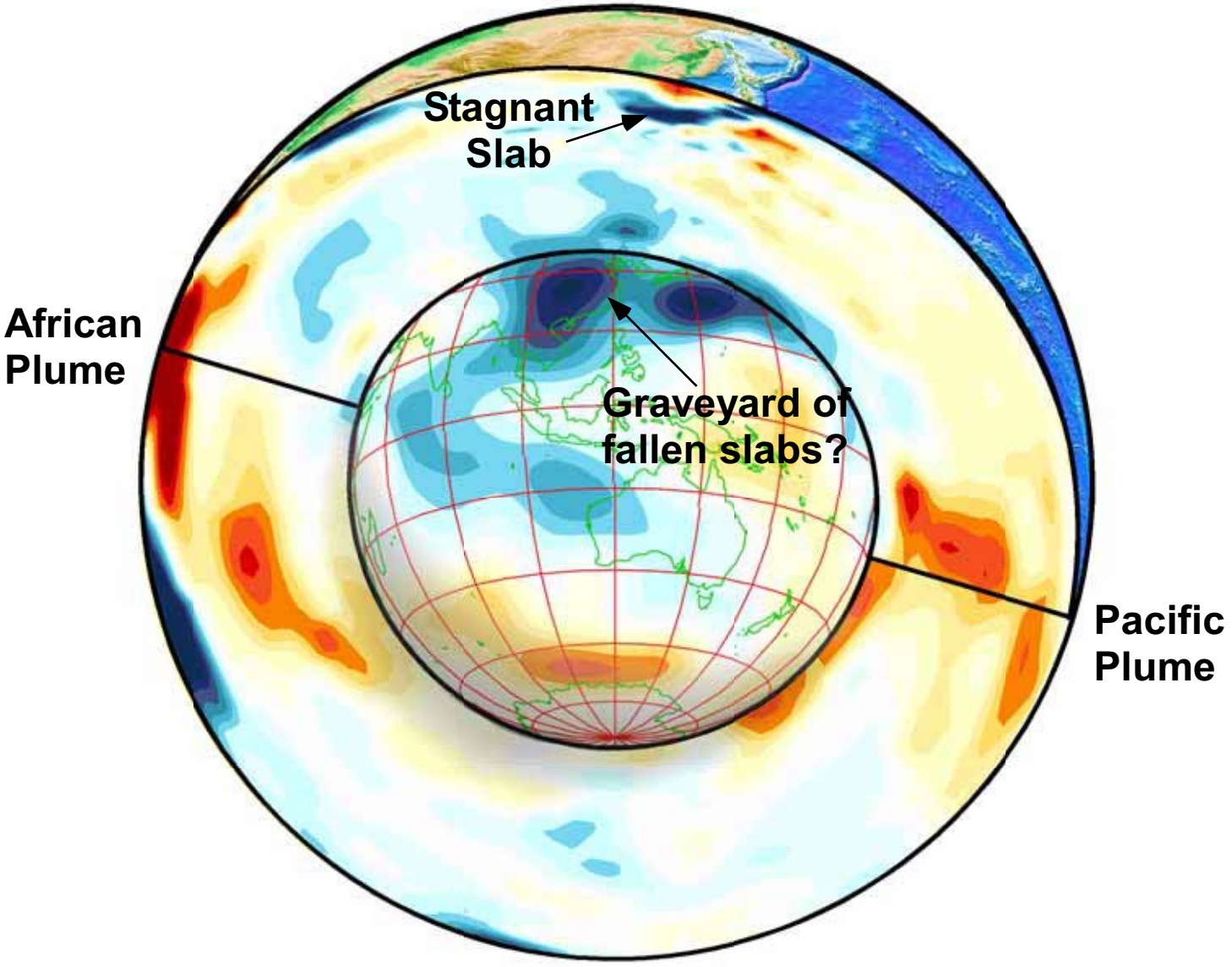

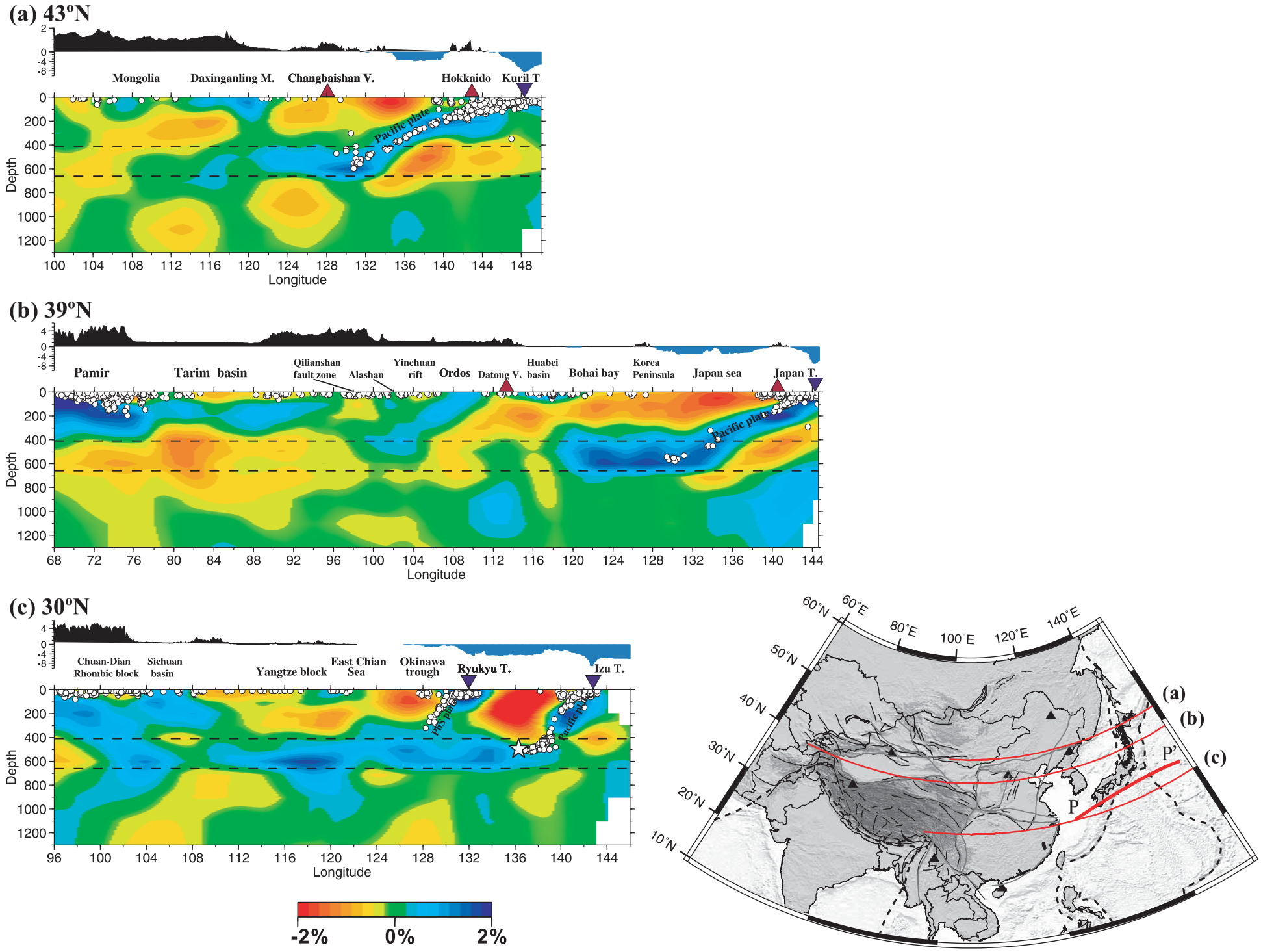
(a) 43°N
Mongolia
Daxinganling M.
Changbaishan V.
Hokkaido
Kuril T.
Pacific plate
Depth
Longitude
(b) 39°N
Pamir
Tarim basin
Qilianshan fault zone
Alashan
Yinchuan rift
Ordos
Datong V.
Huabei basin
Bohai bay
Korea Peninsula
Japan sea
Japan T.
Pacific plate
Depth
Longitude
(c) 30°N
Chuan-Dian Rhombic block
Sichuan basin
Yangtze block
East Chian Sea
Okinawa trough
Ryukyu T.
Izu T.
Pacific plate
Depth
Longitude
-2%
0%
2%
60°N
60°E
80°E
100°E
120°E
140°E
50°N
40°N
30°N
20°N
10°N
(a)
(b)
(c)
P
P'

Fukao et al. Figure 3

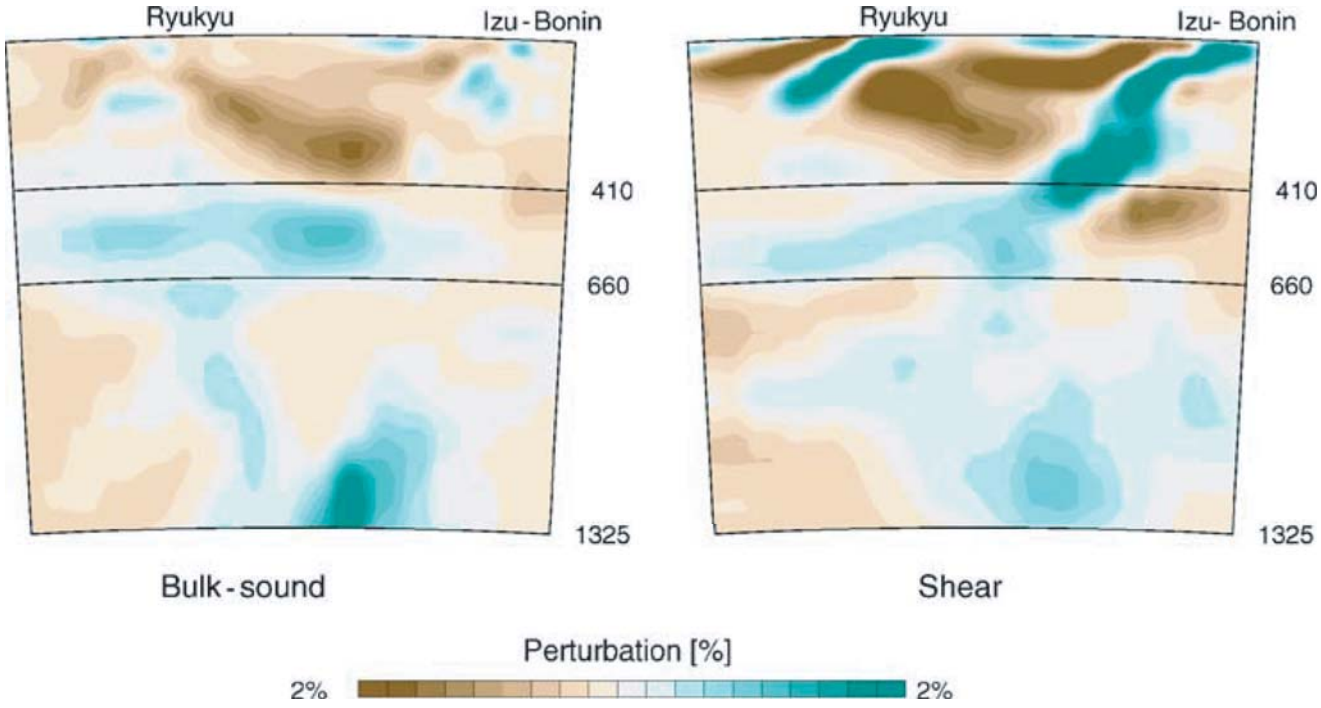

Fukao et al. Figure 4

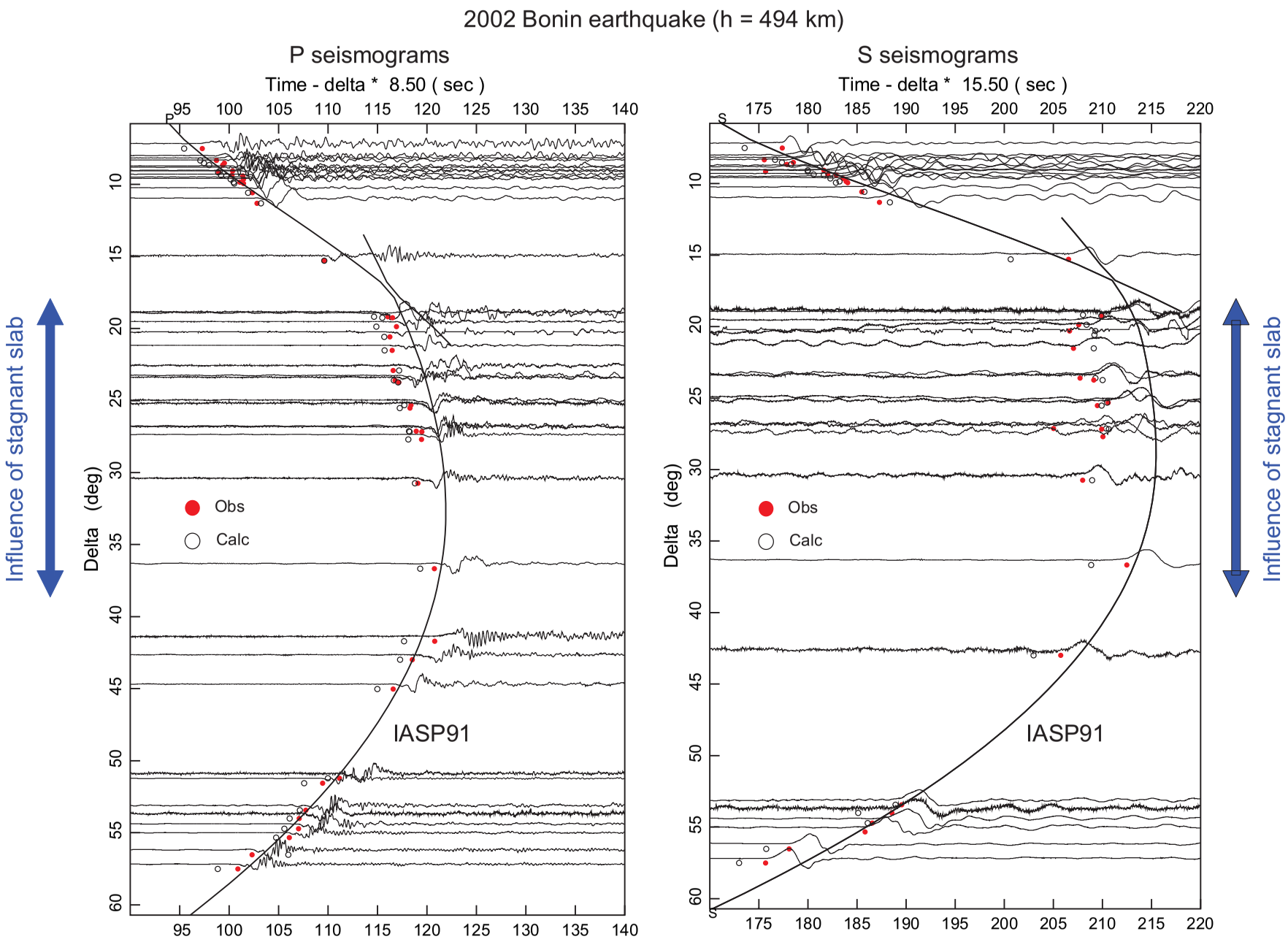

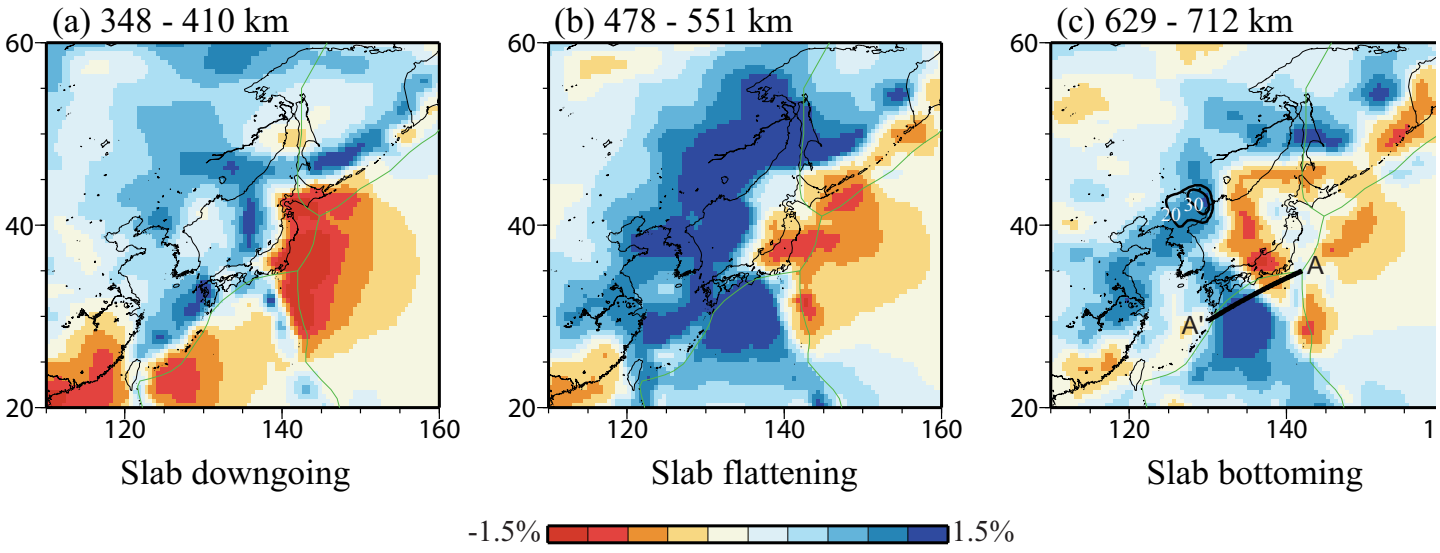
(a) 348 - 410 km
(b) 478 - 551 km
(c) 629 - 712 km
60
40
20
120
140
160
20
30
A
A'
Slab downgoing
Slab flattening
Slab bottoming
-1.5%
1.5%

Fukao et al. FIgure 6

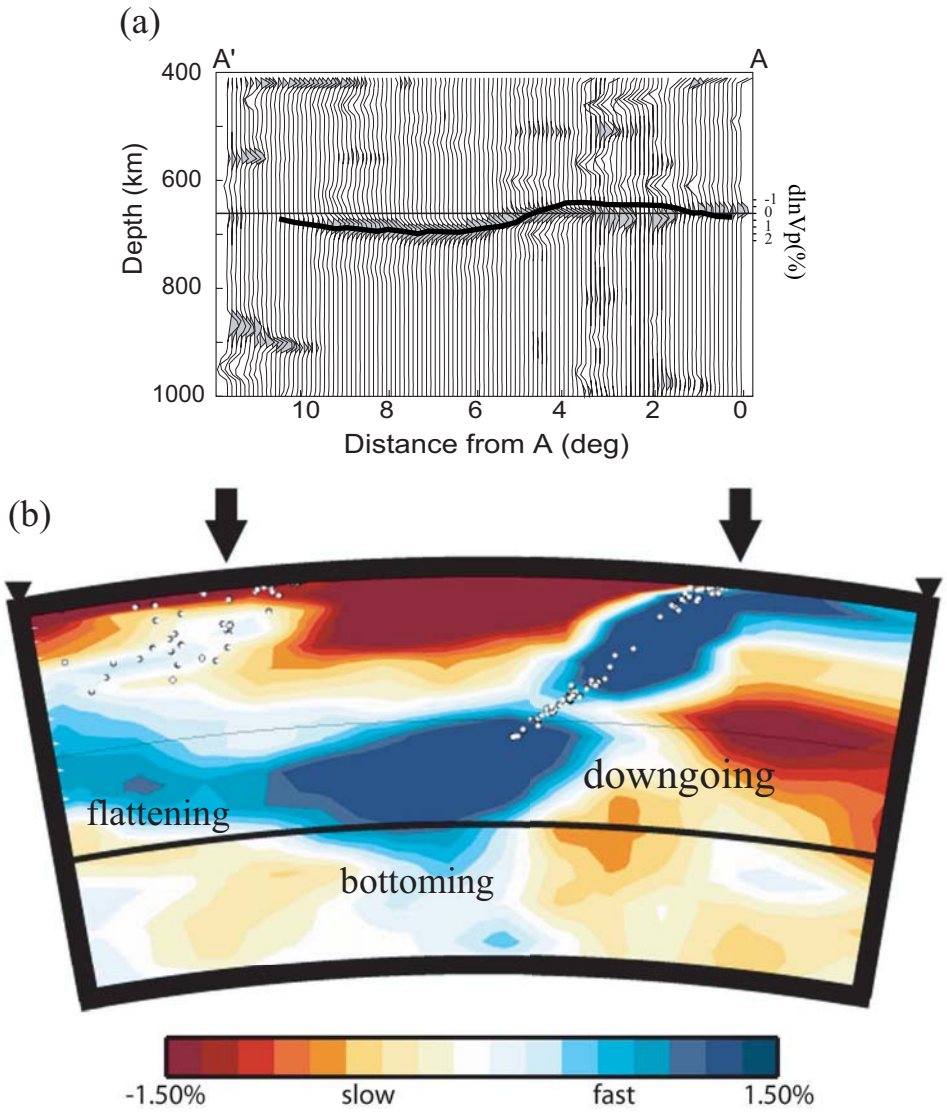

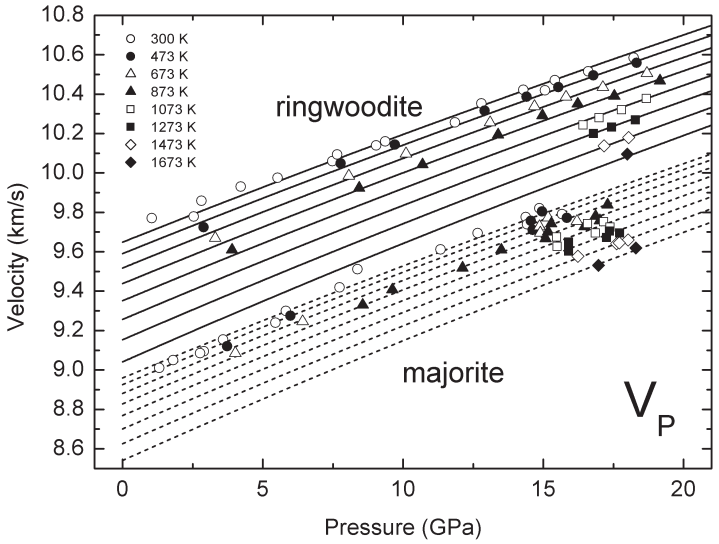

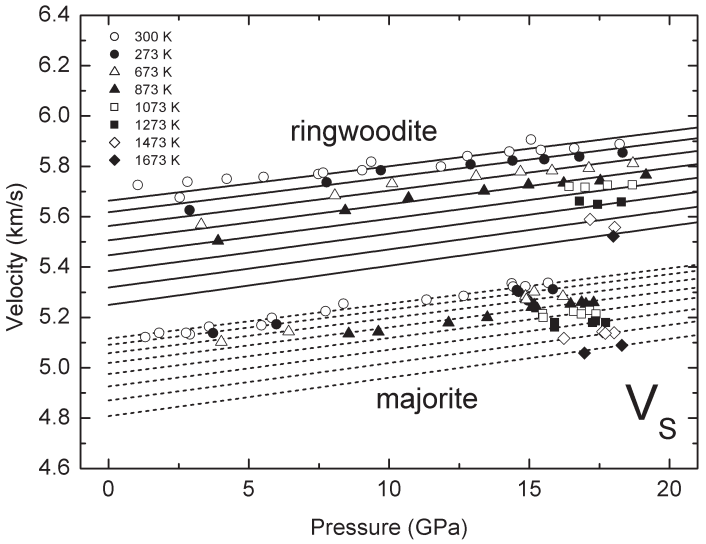

Fukao et al. Figure 7

Fukao et al. Figure 8

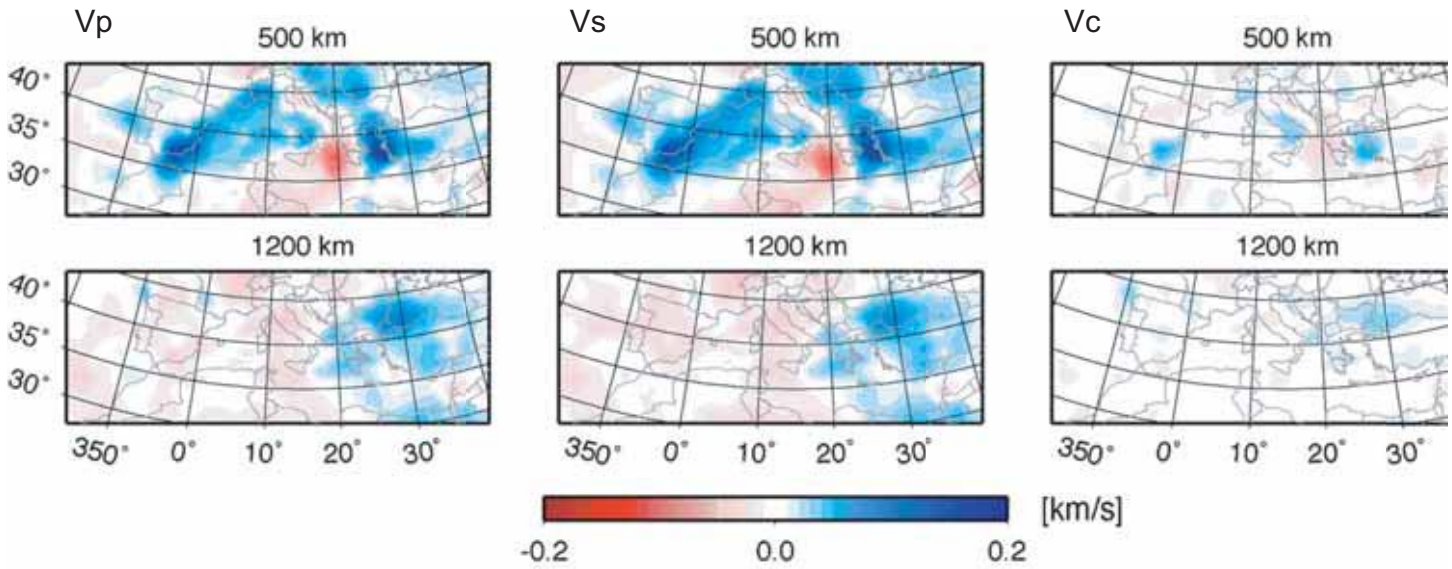

Fukao et al. Fiigure 9

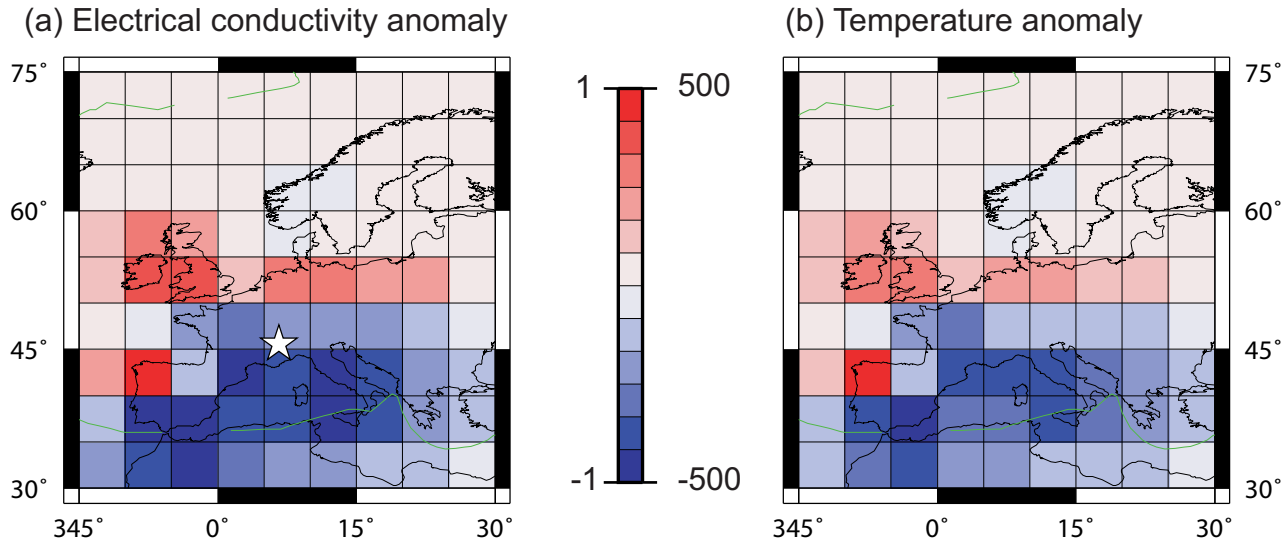

Fukao et al. Figure 10

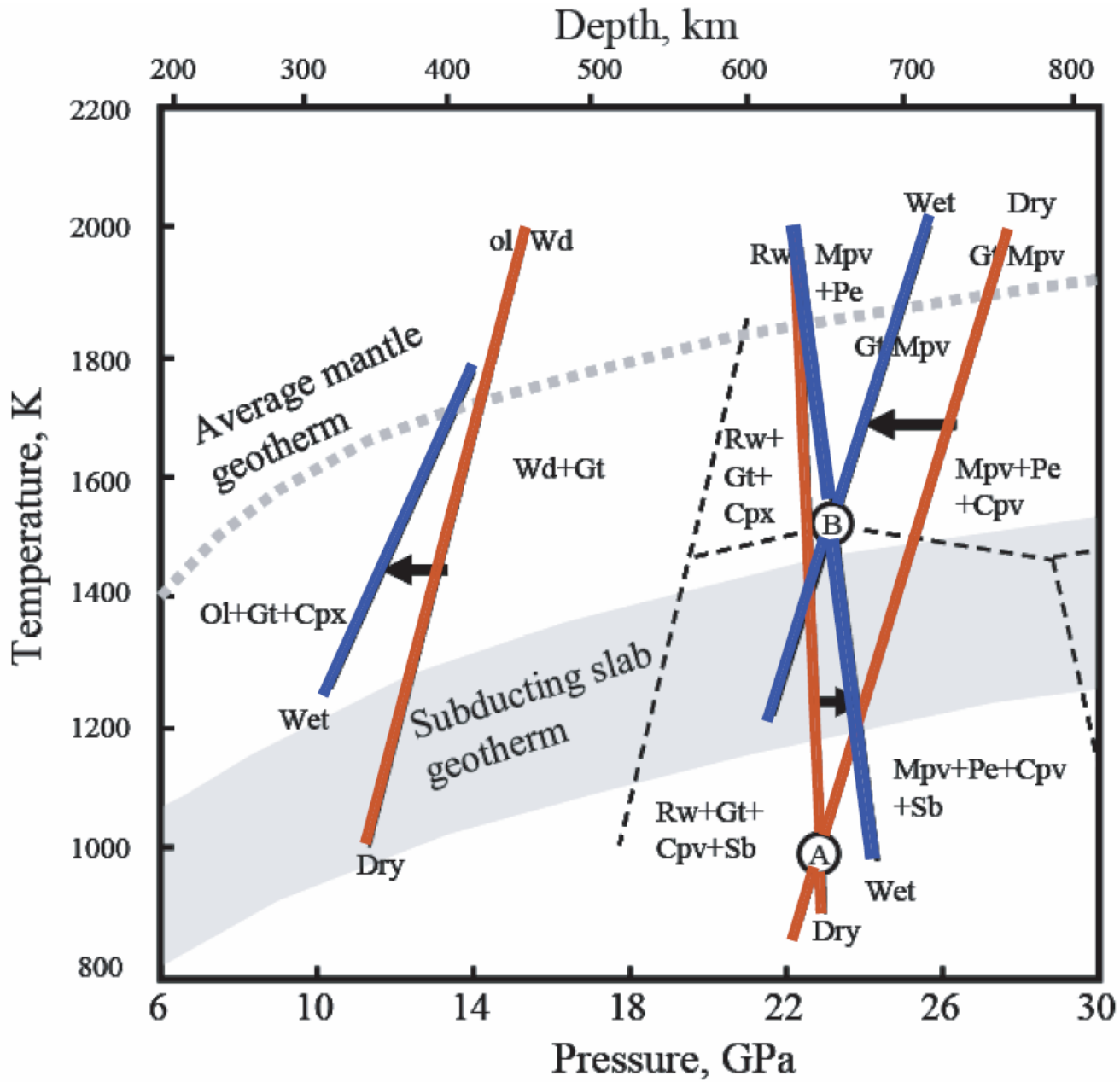

Fukao et al. Figure 11

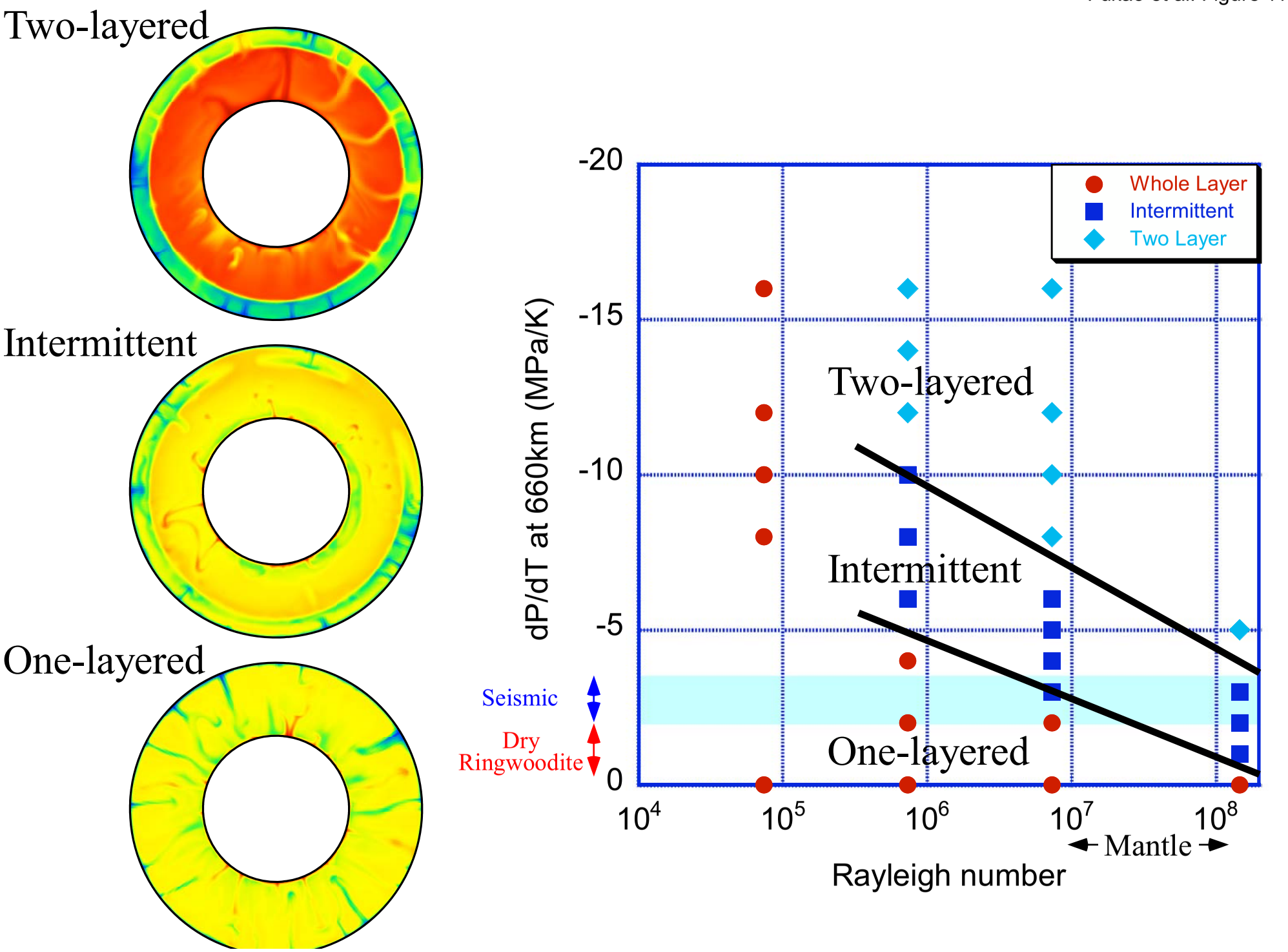

Fukao et al. Figure 12

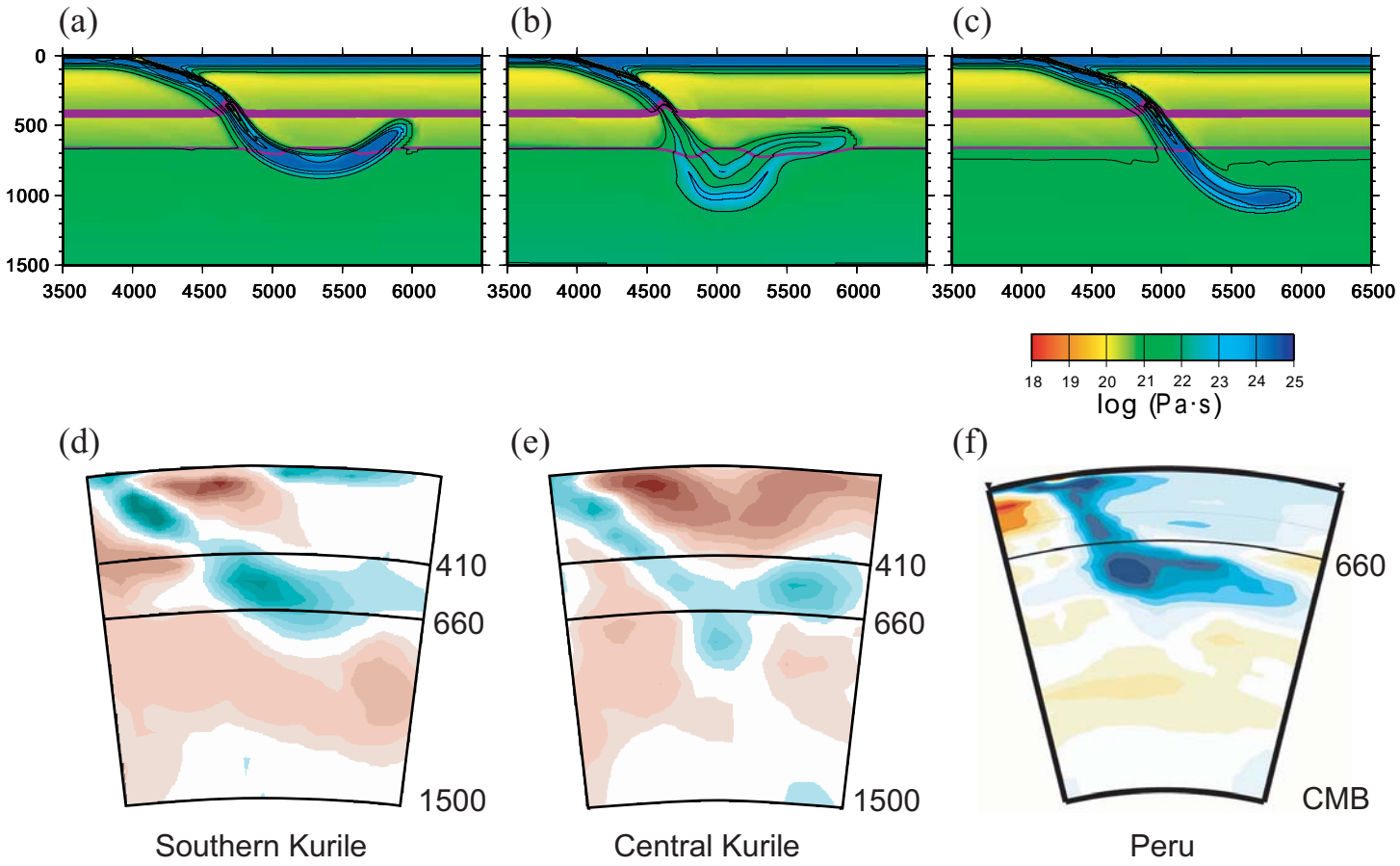

Fukao et al. Figure 13

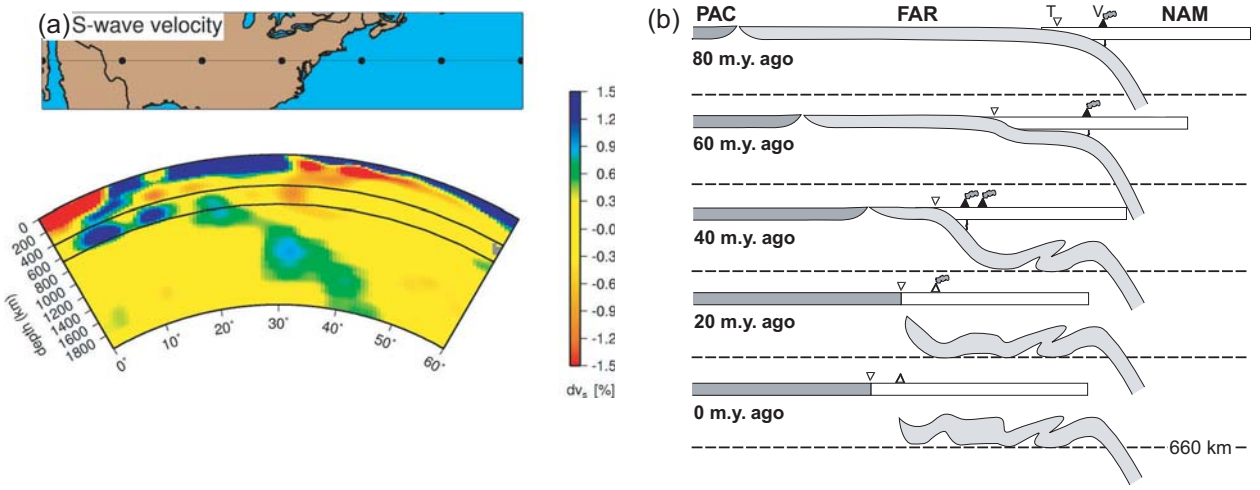

Fukao et al. FIgure 14

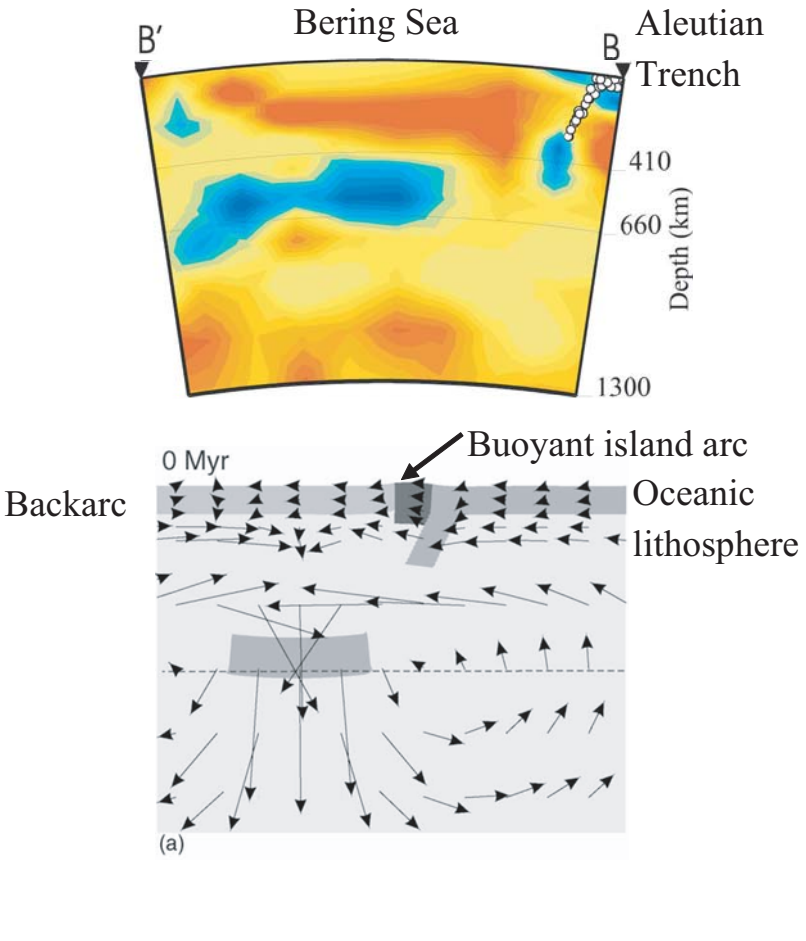

Fukao et al. Figure 15

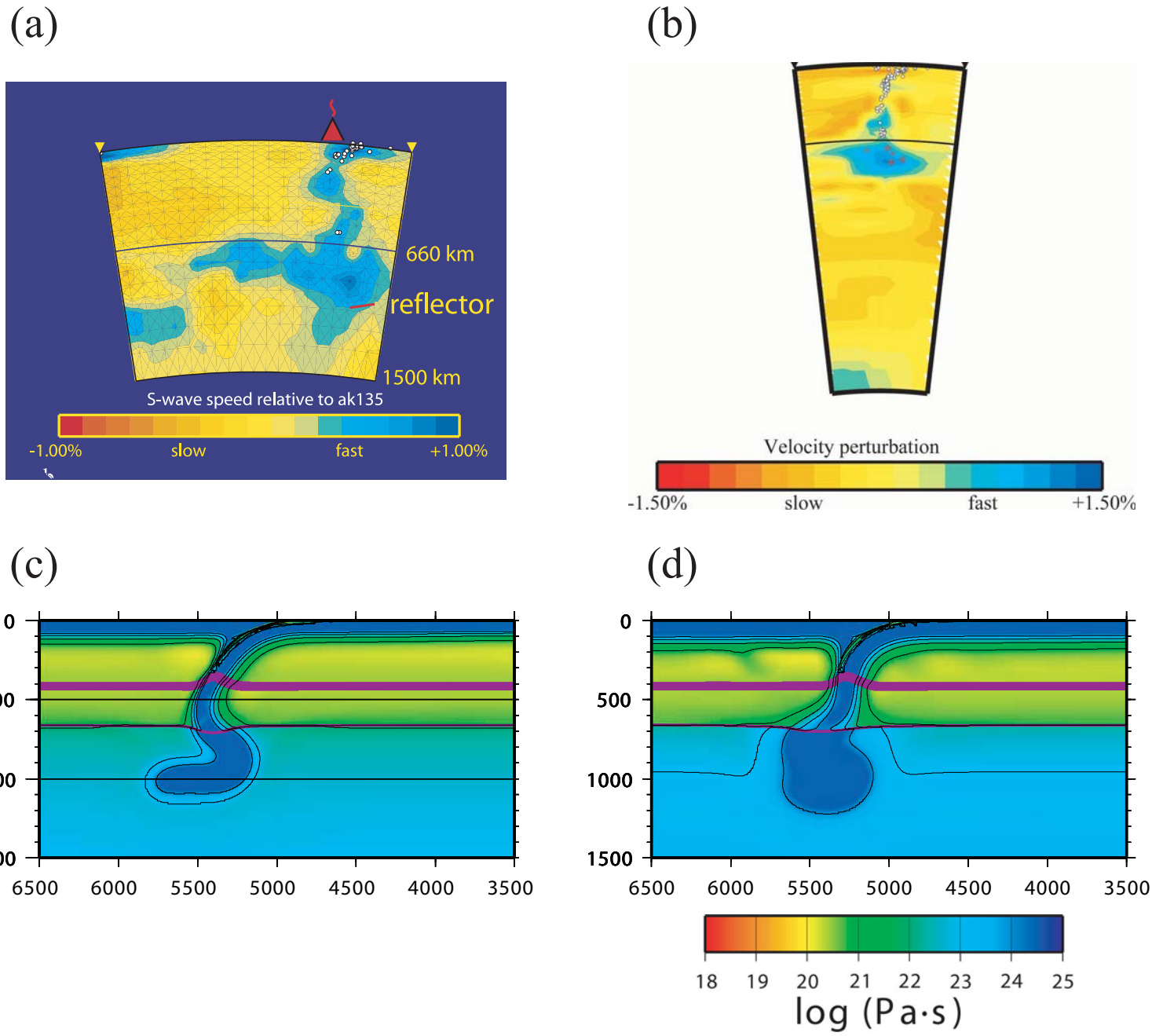

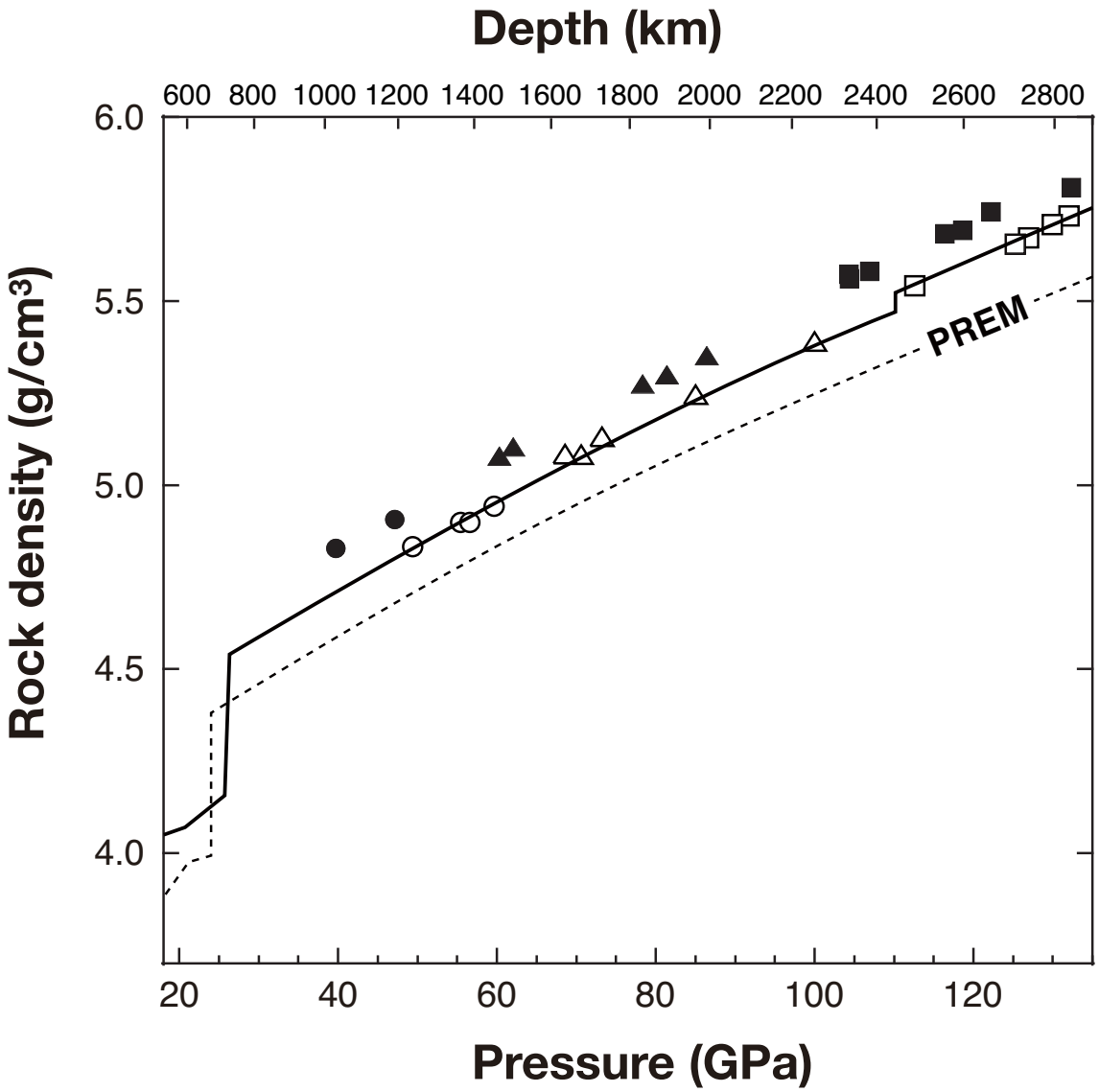

Fukao et al. Figure 16

Fukao et al. Figure 17

(a)

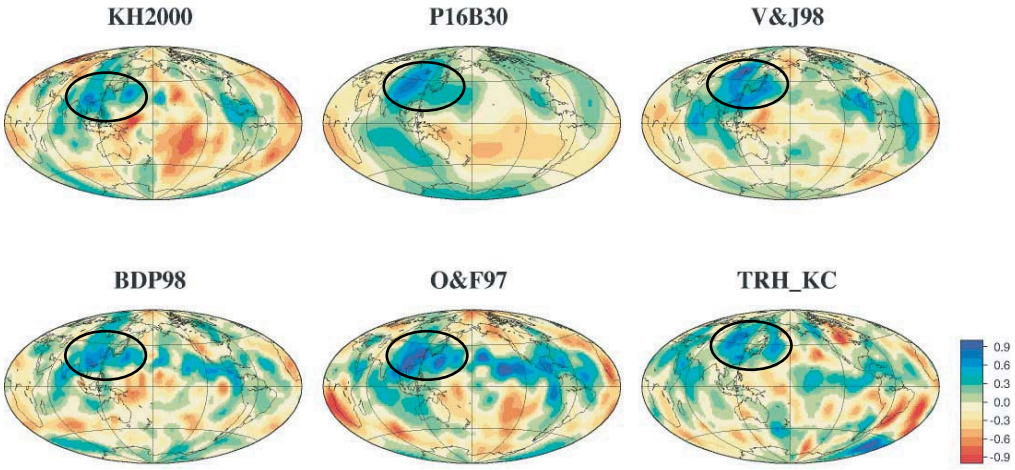

(b)